Energy Reports 11 (2024) 287–303

Contents lists available at ScienceDirect

Energy Reports

journal homepage: www.elsevier.com/locate/egyr

Research paper

Tuning data preprocessing techniques for improved wind speed prediction

Ahmad Ahmad [a], Xun Xiao [b], Huadong Mo [c,*], Daoyi Dong [a,d]

[a] School of Engineering and Technology, University of New South Wales, Canberra, Australia
[b] Department of Mathematics and Statistics, University of Otago, Dunedin, New Zealand
[c] School of Systems and Computing, University of New South Wales, Canberra, Australia
[d] CIICADA Lab, School of Engineering, Australian National University, Canberra, Australia

ARTICLE INFO

Keywords:
Wind speed forecasting
Discrete wavelet transform
Singular spectrum analysis
Time series
Hyperparameter

ABSTRACT

Accurate wind speed forecasting is crucial for efficiently integrating of wind power into the electrical grid and ensuring a stable power supply. However, wind speed is inherently noisy and unpredictable, making it challenging to forecast accurately. This study investigates the effects of hyperparameters of Discrete Wavelet Transform (DWT) and Singular Spectrum Analysis (SSA) on the accuracy of wind speed forecasting using various prediction models. Our proposed method focuses on the optimisation of hyperparameters within the existing models, suggesting that significant untapped potential remains. Our study examines a wide range of wavelet function orders for DWT and varying trend ratio parameter for SSA, and evaluates their impact on the prediction accuracy using real data from thirteen locations in Jordan. Particularly, our investigation reveals that high-order Daubechies wavelets in DWT outperform low-order wavelets. The study also illustrates that optimal hyperparameters must be modified when changing the prediction model and the combination of DWT and SSA enhances prediction performance when the trend ratio is set to 90%. Our results demonstrate that fine-tuning data preprocessing techniques is essential for accurate wind speed prediction since hyperparameter tuning results in greater improvements in prediction accuracy than sophisticated prediction models alone. Our findings underscore the importance of leveraging data preprocessing techniques and hyperparameter tuning for accurate wind speed forecasting.

1. Introduction

1.1. Background

Renewable energy is becoming more and more popular in the global energy grid. Due to the intermittent and unpredictable nature of renewable energy, increasing penetration of photovoltaic and wind systems is causing potential negative impacts on network operation given the power fluctuations generated by these systems (Xu et al., 2021). These can result in unstable operation of the electric network, high power swings in the feeders (Xu et al., 2022), and excessive voltage fluctuations at certain nodes in the grid (Bakos, 2009). Accurate renewable energy forecasting is critical for mitigating the potential risks associated with uncertainties that arise from renewable energy, e.g., grid instability, energy curtailment, extra costs, and compromised reliability (Jones, 2017). It is also beneficial for better planning, management, and operations of electrical power and energy systems (Frías-Paredes et al., 2017). Particularly, accurate renewable energy forecasts can further help reduce imbalance charges and penalties, and give renewable energy providers an advantage in energy market trading. Lastly, accurate forecasts can improve project effectiveness, and they can incorporate more renewable energy into the global energy mix (Lerner et al., 2009).

Global experience has demonstrated that accurate and reliable forecasting systems for wind power are widely agreed as a significant factor in boosting wind penetration (Wu and Hong, 2007). Effective wind speed prediction models facilitate the feasibility study for a potential wind farm site, improve cost savings and worker safety, and minimise the damage caused by severe weather to wind energy systems. Numerous endeavours were made to predict wind speed with sufficient accuracy (Tayal, 2017). However, wind speed forecasting with high accuracy remains a complex and hard issue due to the randomness and transience of wind speed time series (Hu et al., 2018).

1.2. Overview on existing works

The section presents an overview of wind speed prediction models, data preprocessing techniques, and the physical locations of data sources used in wind speed forecasting. The prediction models include

* Corresponding author.
E-mail address: huadong.mo@adfa.edu.au (H. Mo).

https://doi.org/10.1016/j.egyr.2023.11.056
Received 23 May 2023; Received in revised form 29 September 2023; Accepted 28 November 2023
Available online 7 December 2023

physical, statistical, and artificial intelligence models, and their combinations. Data processing techniques include data decomposition, dimensionality reduction, and data correction. This section also discusses different data locations where wind speed data has been collected and analysed for wind speed prediction.

1.2.1. Prediction models

Many models have been used to predict wind speed, and these models can be roughly classified into physical, statistical, artificial intelligence models and their combinations. Before reviewing each category of models, there is a simple benchmark for wind speed forecasting called the persistence approach. This approach makes a simple assumption that the wind speed will not change at the time of the forecast (Zhao et al., 2011). To evaluate any wind speed forecast model, it should first be compared to the persistence method as a baseline (Soman et al., 2010). Physical methods, which are often known as Numerical Weather Prediction (NWP) models, are mathematical models that simulate atmospheric dynamics using physical and mechanical principles with many meteorological and geographical variables. Physical methods use temperature, pressure, roughness, and topography to forecast weather conditions for a large-scale area. These methods need a large amount of computational resources and are thus reserved for long-term forecasting horizons (Sweeney et al., 2020). Therefore, physical methods are inappropriate for short-term forecasting at a single location (Lei et al., 2009; Wang et al., 2019a). Many researchers predicted wind speed using statistical models such as AutoRegressive Integrated Moving Average (ARIMA) (Palomares-Salas et al., 2009; Singh et al., 2019), Markov Chain model (Wang et al., 2015), Quantile Regression (QR) (Nielsen et al., 2006; Haque et al., 2014), and Bayesian approach (Wang et al., 2019b; Blonbou, 2011). The objective of the statistical models is to investigate the relationship between the past historical wind speed and the future wind speed during the next few hours in order to make predictions and address the associated uncertainty. However, due to the random and nonlinear nature of wind speed time series, these statistical methods are often inapplicable for accurately depicting the properties of wind speed time series (Jiang et al., 2021). In order to deal with the nonlinearity of wind speed, many studies deployed machine learning techniques, e.g., Support Vector Regression (SVR) (Chen and Yu, 2014), Gaussian Process Regression (GPR) (Zhang et al., 2016), and Artificial Neural Network (ANN) (Cadenas and Rivera, 2009). Different forms of ANNs with specific characteristics have been extensively studied and evaluated in the literature, which are designed to deal with data with noisy and irregular patterns, including Generalised Regression Neural Network (GRNN) (Kumar and Malik, 2016), and Wavelet Neural Network (WNN) (Doucoure et al., 2016; Santhosh et al., 2018; Chitsaz et al., 2015), Recurrent Neural Networks (RNN) (Graves et al., 2008; Ardalani-Farsa and Zolfaghari, 2010), Elman Neural Network (ENN) (Wu and Lundstedt, 1996), and Nonlinear AutoRegressive eXogenous Neural Network (NARX) (Jawad et al., 2018; Saha and Chauhan, 2017), resulting in improved prediction accuracy. In addition, different prediction models was combined to integrate the advantages of individual models, such as ARIMA-ANN hybrid model (Liu et al., 2012; Cadenas and Rivera, 2010), and ANN-SVR hybrid model (Khosravi et al., 2018).

1.2.2. Data preprocessing techniques

The papers reviewed in Section 1.2.1 have demonstrated the capacity of many prediction models to reduce prediction errors, but there is still potential for further improvement. In light of that, different data preprocessing techniques were employed to enhance the prediction accuracy. The data processing techniques may mainly be divided into three classes, i.e., data decomposition, dimensionality reduction, and data correction (Liu and Chen, 2019). Generally, data decomposition, such as Wavelet Decomposition (WD) (Lei and Ran, 2008; An et al., 2011; Mandal et al., 2014), Empirical Mode Decomposition (EMD) (Wang et al., 2016), Variational Mode Decomposition (VMD) (Naik et al., 2018), is used to decompose the original series into a number of relatively stationary subseries, so as to ease the difficulty of forecasting. Dimensionality reduction, which comprises feature selection and extraction, employs methods such as autocorrelation analysis (Hu et al., 2018) and principal component analysis (Davò et al., 2016) to minimise input dimensionality. Data correction encompasses a range of processes, including data denoising, residual error modelling, outlier detection, and filter-based rectification. Data denoising techniques, such as Singular Spectrum Analysis (SSA) (Liu et al., 2018) and Wavelet threshold denoising (Mi et al., 2017), are utilised to eliminate noise from input datasets.

Discrete Wavelet Transform (DWT) and SSA are chosen for our numerical study given their specialised capabilities in handling wind speed time series and effective feature extraction, which makes them ideal choices for improving forecasting accuracy. Liu et al. (2014) used a model combining DWT with Support Vector Machine (SVM), and the results showed the prediction error is reduced. Zhang et al. (2022a) examined a model integrating DWT, Seasonal Autoregressive Integrated Moving Average (SARIMA), and Long short-term memory (LSTM) to forecast wind power with enhanced prediction accuracy. Catalão et al. (2011) combined ANN with DWT to forecast the wind speed and the proposed model outperformed the persistence model, ANN without DWT, and ARIMA. Mi and Zhao (2020) examined SSA and modified adaptive structural learning of neural network, then combined these techniques with LSTM. Wang et al. (2020b) tested a hybrid Laguerre neural network with SSA. Moreno and dos Santos Coelho (2018) suggested a hybrid approach that combines SSA and the Adaptive Neuro Fuzzy Inference System.

Furthermore, the combination of different preprocessing techniques has been tested by many authors. Yin et al. (2019) used a cascaded Convolutional Neural Network-LSTM wind power prediction strategy with EMD-VMD preprocessing techniques and the results demonstrated that this prediction model reduces the forecasting error. Liu et al. (2018) suggested a combination of preprocessing techniques, specifically VMD and SSA, in conjunction with prediction models, including LSTM and Extreme Learning Machine. Yu et al. (2017) examined the combination of DWT and SSA to denoise the high frequency sub-series, and integrated it with ENN for wind speed prediction. The results demonstrated that this combination outperforms other approaches in terms of prediction accuracy.

1.2.3. Data locations

Wind behaviour is greatly influenced by topography and climate, which differ from place to place (Castellani et al., 2015) . High slopes can accelerate air currents, and extreme weather conditions can affect wind flow (Castellani and Franceschini, 2005). According to the existing studies, it can be seen that the majority of prior studies validated their approaches using real data from China. There are also a lot of papers examining the performance of prediction models using datasets from other countries such as the United States, Brazil, Iran, Australia, etc., as shown in Table 1.

1.3. Research gaps and contributions

According to the aforementioned literature, the improvement of prediction models may be ascribed to the utilisation of advanced models, such as statistical models and machine learning approaches, as well as the implementation of data preprocessing techniques, including DWT, SSA, EMD, and VMD. The prior studies (Lei and Ran, 2008; An et al., 2011; Mandal et al., 2014; Wang et al., 2016; Naik et al., 2018; Hu et al., 2018; Davò et al., 2016; Liu et al., 2018; Mi et al., 2017; Liu et al., 2014; Zhang et al., 2022a; Catalão et al., 2011; Mi and Zhao, 2020; Wang et al., 2020b; Moreno and dos Santos Coelho, 2018; Yin et al., 2019; Yu et al., 2017) showed that the data preprocessing techniques can improve prediction performance. However, few publications have investigated the optimal hyperparameters of these data preprocessing

Table 1
Locations of datasets used for wind speed forecasting.

Country	No. of datasets	Reference
China	15	Hu et al. (2018), Wang et al. (2015, 2019b), Zhang et al. (2016), Liu et al. (2012), An et al. (2011), Wang et al. (2016) and Liu et al. (2018) Li et al. (2018), Liu et al. (2014), Mi and Zhao (2020), Wang et al. (2020b), Yu et al. (2017), Liu et al. (2013) and Zhang et al. (2013)
USA	5	Haque et al. (2014), Jawad et al. (2018), Naik et al. (2018), Tascikaraoglu et al. (2016) and Kiplangat et al. (2016)
Spain	4	Frías-Paredes et al. (2017), Palomares-Salas et al. (2009), Yin et al. (2019) and Zhang et al. (2022b)
Canada	3	Doucoure et al. (2016), Chitsaz et al. (2015) and Mandal et al. (2014)
India	3	Kumar and Malik (2016), Santhosh et al. (2018) and Jaseena and Kovoor (2020)
Mexico	3	Cadenas and Rivera (2007, 2009) and Cadenas and Rivera (2010)
Brazil	2	Saha and Chauhan (2017) and Moreno and dos Santos Coelho (2018)
Italy	2	Davò et al. (2016) and Castellani et al. (2015)
Australia	1	Tayal (2017)
Denmark	1	Nielsen et al. (2006)
France	1	Blonbou (2011)
Greece	1	Barbounis et al. (2006)
Iran	1	Khosravi et al. (2018)
Ireland	1	Singh et al. (2019)
Portugal	1	Catalão et al. (2011)
Scotland	1	Zhang et al. (2022a)

Table 2
Different literature used DWT for wind forecasting.

Reference	Wavelet function and its order	Decomposition level
Lei and Ran (2008)	Daubechies, 5th order	6
Liu et al. (2014)	Daubechies, 4th order	2
Zhang et al. (2022a)	Daubechies, 3rd order	2
Catalão et al. (2011)	Daubechies, 4th order	3
Yu et al. (2017)	Daubechies, 6th order	3
Liu et al. (2013)	Are not mentioned	3
Zhang et al. (2013)	Daubechies, 3rd order	1
Tascikaraoglu et al. (2016)	Daubechies, 4th order	2
Kiplangat et al. (2016)	Daubechies, 8th order	11

techniques that lead to the most accurate wind speed forecasts. For example, the majority of studies employed the Daubechies wavelet function with an order between 3 and 8 and a decomposition level of 2 to 3 as indicated in Table 2. Moreover, they relied on other studies for determining DWT hyperparameters, such as precipitation forecasting (Zhang et al., 2022a), load forecasting (Tascikaraoglu et al., 2016), and detection of ice accretion on wind turbines (Yu et al., 2017). The hyperparameters are often chosen without good justifications (Liu et al., 2014; Catalão et al., 2011; Liu et al., 2013; Kiplangat et al., 2016).

On the other hand, the interactions between the hyperparameters of data preprocessing techniques, the data, and the prediction models have not been explored. The majority of existing literature evaluated models using a limited number of datasets or tested the models using selected datasets from a particular location. From the literature reviewed, it can be seen that there are limited studies having explored and evaluated the effectiveness of prediction models in the Middle East. In order to address these challenges, a comprehensive numerical study is conducted by incorporating two popular preprocessing techniques, i.e., DWT and SSA, into four representative prediction models, i.e., GPR, SVR, WNN, and LSTM. Particularly, this study identifies the sensitivity of tuning the hyperparameters on the performance of prediction models. This study further tests the prediction models using real datasets from 13 different locations in Jordan, a representative country from the Middle East. This study also examines if the hyperparameters of data preprocessing techniques are associated with the data and/or the prediction model.

The main contributions in this paper can be summarised as follows:

- Investigating the optimal hyperparameters of data preprocessing techniques in DWT and SSA for wind speed forecasting in combination with various prediction models, including WNN, SVR, LSTM, and GPR, and comparing them with the findings of previous studies.
- Identifying the sensitivity of tuning hyperparameters of data preprocessing techniques and examining the impact of high DWT wavelet function orders with varying decomposition levels on the forecasting performance. This contributes to the optimisation of data preprocessing techniques and the improvement of wind speed forecasting accuracy.
- Exploring the linkages between the hyperparameters of data preprocessing techniques, the data, and the prediction models. This contributes to a better understanding of the underlying mechanisms and interactions between the prediction models and data preprocessing techniques.
- Evaluating the effectiveness of adopting the optimal hyperparameters of data preprocessing techniques when combining SSA and DWT.
- Conducting a case study for various Jordanian locations and analysing the performance of prediction models and their ability to predict wind speed.

The remainder of the article is structured as follows. Section 2 briefly introduces the selected prediction models and data preprocessing techniques. In Section 3, a description of the datasets, and a detailed explanation of the methodology are presented. Section 4 presents and discusses the performance of various prediction models with different preprocessing techniques through a case study based on real data. Section 5 discusses the implications and insights derived from these findings, and Section 6 provides a conclusion of the study.

2. Preliminary work

This section describes the basic formulation of DWT and SSA used in this paper, as well as the reasons for selecting WNN, SVR, GPR, and LSTM as the prediction models in this investigation.

2.1. Preprocessing techniques

The first data preprocessing technique utilised in this investigation is DWT. DWT is a transform that divides a given signal into a number of sets, each of which is a time series of coefficients characterising the signal's time evolution in the corresponding frequency band (Han et al., 2012). DWT is the digital equivalent of the continuous wavelet transform, but requires less computation and provides nearly the same precision. DWT involves several steps (Mallat, 1989), beginning with the selection of an appropriate wavelet function. Once the wavelet function is chosen, a low-pass filter is applied to the input signal to extract its low-frequency components, as represented by the following equation:

$$a_1[j] = \sum_t Y[t]h[j-2t], \qquad j = 0, 1, \ldots, \frac{N}{2} - 1 \tag{1}$$

where $a_1[j]$ represents the approximation coefficients obtained after the low-pass filtering of the signal, $h[j]$ represents the coefficients of the low-pass filter, $Y[t]$ represents the input signal, t represents the position of each observation in the input signal, and N represents the length of the signal. Next, a high-pass filter is applied to the input signal to

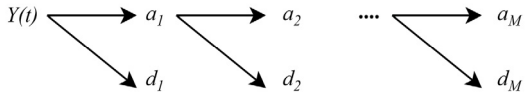

Fig. 1. The process of DWT.

extract its high-frequency components, as represented by the following equation:

$$d_1[j] = \sum_t Y[t]g[j-2t], \qquad j = 0, 1, \ldots, \frac{N}{2} - 1 \tag{2}$$

where $d_1[j]$ represents the detail coefficients obtained after the high-pass filtering of the signal, $g[j]$ represents the coefficients of the high-pass filter. These two steps are repeated iteratively on the low-frequency component obtained from the previous step until the desired level of decomposition is achieved, as represented by the following equations:

$$a_m[j] = \sum_t a_{m-1}[t]h[j-2t], \qquad j = 0, 1, \ldots, \frac{N}{2^m} - 1 \tag{3}$$

$$d_m[j] = \sum_t a_{m-1}[t]g[j-2t], \qquad j = 0, 1, \ldots, \frac{N}{2^m} - 1 \tag{4}$$

where $a_m[j]$ and $d_m[j]$ represent the approximation and detail coefficients at the mth level of decomposition. The whole process can be summarised in Fig. 1. In this study, the Daubechies wavelet is used as the wavelet function. The scaling functions for Daubechies wavelets provide compact support and, more crucially, can be used to decompose and reconstruct polynomial functions effectively.

SSA is the second data preprocessing technique to be implemented in this investigation. SSA is a nonparametric method for time series analysis, capable of identifying and extracting trends, periodic oscillation, and noise components from the original series (Moreno and dos Santos Coelho, 2018). The SSA algorithm has two stages, which are called decomposition and reconstruction (Golyandina et al., 2001). Two critical factors are relevant in the SSA process: the window length and the trend ratio. The basic idea of SSA is to form a trajectory matrix from the time series by embedding the time series into a higher dimensional space (Elsner and Tsonis, 1996). The trajectory matrix is then decomposed using singular value decomposition (SVD) to obtain the empirical modes. The first step in SSA is to choose a window length, which determines the number of embedded dimensions. The window length (L) must be an integer within the range $2 \le L \le \frac{N-1}{2}$. The work (Wang et al., 2020b; Moreno and dos Santos Coelho, 2018) proposed an equation to compute the window length, which can be computed by dividing the length of the wind time series over the number of samples observed during one hour. On the other hand, the trend ratio (TR) is an important measure for assessing the significance of trends in the time series, as it can help distinguish between a true trend and random fluctuations in the data (Elsner and Tsonis, 1996). A high trend ratio indicates a strong trend, while a low trend ratio suggests that the trend component is weak compared to other sources of variability in the data (Golyandina et al., 2001). Therefore, the trend ratio is the tuning parameter of SSA and will be further investigated in this paper. The trend ratio can be determined as follows (Yu et al., 2017):

$$TR = \frac{\sum_i^K \lambda_i}{\sum_i^L \lambda_i} \tag{5}$$

where λ_i are the singular values obtained from SVD of the trajectory matrix in SSA, K is the number of singular values considered to represent the trend, and L is the total number of singular values, which equals the window length.

Fig. 2. Locations of wind measuring.

2.2. Prediction models

Four different prediction models are included in the study: WNN, SVR, GPR, and LSTM. WNN is implemented as suggested by Alexandridis and Zapranis (2013) with Adam optimiser. Also, a linear link is established between the neurons and the output node. To increase the forecasting accuracy, direct input-to-output connections (DIOCs) are implemented (Pao et al., 1994; Peng et al., 1992; Ren et al., 2016; Wang et al., 2020a). Moreover, the Morlet wavelet function is used because it produces a more accurate wind power forecast than the Mexican-hat wavelet function (Chitsaz et al., 2015). SVR is the second prediction model. In this paper, SVR is chosen since it takes significantly less computing time than ANN. GPR is chosen since it is an intelligent regression technique based on Bayesian theory. It combines both the reasoning ability of Bayesian networks and the adaptability of SVM to address complex problems with small sample sizes, high dimensions, and substantial nonlinearities (Zhang et al., 2022b). LSTM is the fourth prediction model, which is one of the significant deep learning architectures. It is capable of long term memory tasks with more time steps. It has an internal memory state, which significantly reduces the multiplication effects of small/large gradients and thus reduces the vanishing gradient problems (Jaseena and Kovoor, 2020). It is implemented with Adam optimiser.

3. Methodology

3.1. Data description

The case study covers 13 different Jordanian sites. As illustrated in Fig. 2, these sites were chosen to represent as much of the country as possible. The data is collected from the National Energy Research Centre (NERC)/Royal Scientific Society (RSS). Table 3 highlights the name, coordinates, measuring height, time span of data collection, and average wind speed at each location. Notably, these stations were equipped with calibrated anemometers in accordance with ISO17025 and the European standard IEC 61400-12-1 in order to monitor wind speed as part of the wind energy assessment. In addition, each dataset contains the wind speed over one year and the sampling interval for data is 10 min.

Moreover, all datasets are normalised in order to generate high-quality data that can be fed into the learning models. Because wind speed time series data can contain a broad range of values, it must be scaled to encompass the same range of values to accelerate the learning process. Any learning algorithm's efficacy is highly dependent on the normalisation approach used (Nayak et al., 2014). Min–max

Table 3
Information of wind speed data locations.

No.	Location name	Coordinates (WGS84)	Measuring height (m)	Time span of data collection	Average wind speed (m/s)
1	Al Reesheh	E 39.01161°, N 32.57046°	50.0	01/01/2009–31/12/2009	7.04
2	Al Ashqaf	E 37.62118°, N 32.34091°	45.0	01/01/2008–31/12/2008	6.51
3	Tal Al Hassan	E 36.75892°, N 31.96888°	50.0	24/04/2016–23/04/2017	6.34
4	Emm Ejmal	E 36.40417°, N 32.33150°	45.6	05/07/2007–04/07/2008	6.12
5	JUST	E 35.98748°, N 32.48417°	60.0	01/01/2010–31/12/2010	4.74
6	Kamsheh	E 35.89081°, N 32.15304°	50.0	01/01/2009–31/12/2009	6.48
7	Al Alia	E 36.08609°, N 31.86221°	49.0	01/01/2010–31/12/2010	6.23
8	Swaqa	E 36.09023°, N 31.42546°	50.0	20/09/2012–19/09/2013	6.39
9	Al Fujeij	E 35.57063°, N 30.57063°	70.0	01/11/2015–31/10/2016	6.88
10	Al Jafer	E 36.24317°, N 30.52205°	49.0	02/06/2010–01/06/2011	6.04
11	Maan	E 35.68627°, N 30.26091°	51.6	01/01/2010–31/12/2010	6.03
12	Batn Al Ghoul	E 35.91569°, N 29.75743°	50.0	23/09/2010–22/09/2011	5.03
13	Al Aqaba	E 34.98528°, N 29.54379°	45.0	01/01/2003–31/12/2003	6.33

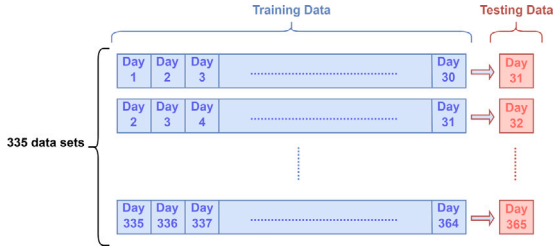

Fig. 3. Rolling-window technique.

normalisation is used in this paper that scales the input values into the range $[0, 1]$, by using the formula:

$$X_{\text{norm}} = \frac{X - X_{\min}}{X_{\max} - X_{\min}} \tag{6}$$

where $X_{\min}$ and $X_{\max}$ are the minimum and maximum values of attribute X of the input dataset.

3.2. The procedure of investigation

For the first step, the data is prepared by the rolling-window technique. Each window is 31 days in length. The first 30 days are used to train the prediction model, and the last day is used to validate the model as shown in Fig. 3. Upon completion of the rolling-window technique, 335 rolling datasets are generated and evaluated. The aim of using the rolling-window technique is to assess the stability and reliability of the selected hyperparameters.

The numerical study begins with prediction models without data preprocessing techniques. Then, the prediction models are combined with DWT, where the wavelet function order will be varying from 1 to 38 and the decomposition level from 1 to 5 in order to study the effectiveness of the DWT hyperparameters on the accuracy of prediction models. Following that, SSA is merged with the optimal wavelet function order and decomposition level, as determined by the prior DWT analysis and it is applied to the highest frequency subseries D_1. DWT and SSA are further combined with the prediction models. During the investigation, the trend ratio TR of SSA is tuned. Fig. 4 summarises the overall methodology.

In this study, N is the length of the highest frequency sub series D_1, as determined by DWT. The sampling interval for wind series data is 10 min, giving six samples per hour. The total number of singular values resulting from SSA is 15, and the study tests four different values of the trend ratio, including 10%, 70%, 80%, and 90% to reconstruct the original highest frequency subseries D_1 while considering the remaining components as noise components. The choice of assessing the data at 10%, 70%, 80%, and 90% of TR is deliberate and rooted in

Fig. 4. Flowchart of the methodology.

analytical considerations. The 10% threshold acts as a foundational marker, highlighting base-level trend contributions, which is vital for understanding series with faint or emergent trends. The 70% threshold is a node to a widely accepted analytical benchmark, often capturing substantial trend dynamics without the convolution of noise. Moving to the 80% threshold, we venture into capturing more nuanced, intricate patterns, ensuring that subtle, yet potentially pivotal, trends are not sidelined. Finally, at 90%, we delve deep into the series' intricacies, aiming for a nearly exhaustive trend capture. This layered approach ensures not only the breadth of analysis, from weak to dominant trends but also a depth that encapsulates both overt and covert trend nuances. Such granularity is essential for offering a holistic, multi-dimensional perspective on the role and manifestation of trends in time series data.

4. Case study

In this section, we present the findings of the case study utilising real datasets. Six different evaluation criteria are employed to evaluate the prediction accuracy as shown in Eqs. (7) to (12), including the Mean Square Error (MSE), the Mean Absolute Error (MAE), the Mean Absolute Percentage Error (MAPE), the Mean Percentage Error (MPE), the coefficient of determination (R^2), and the Pearson correlation

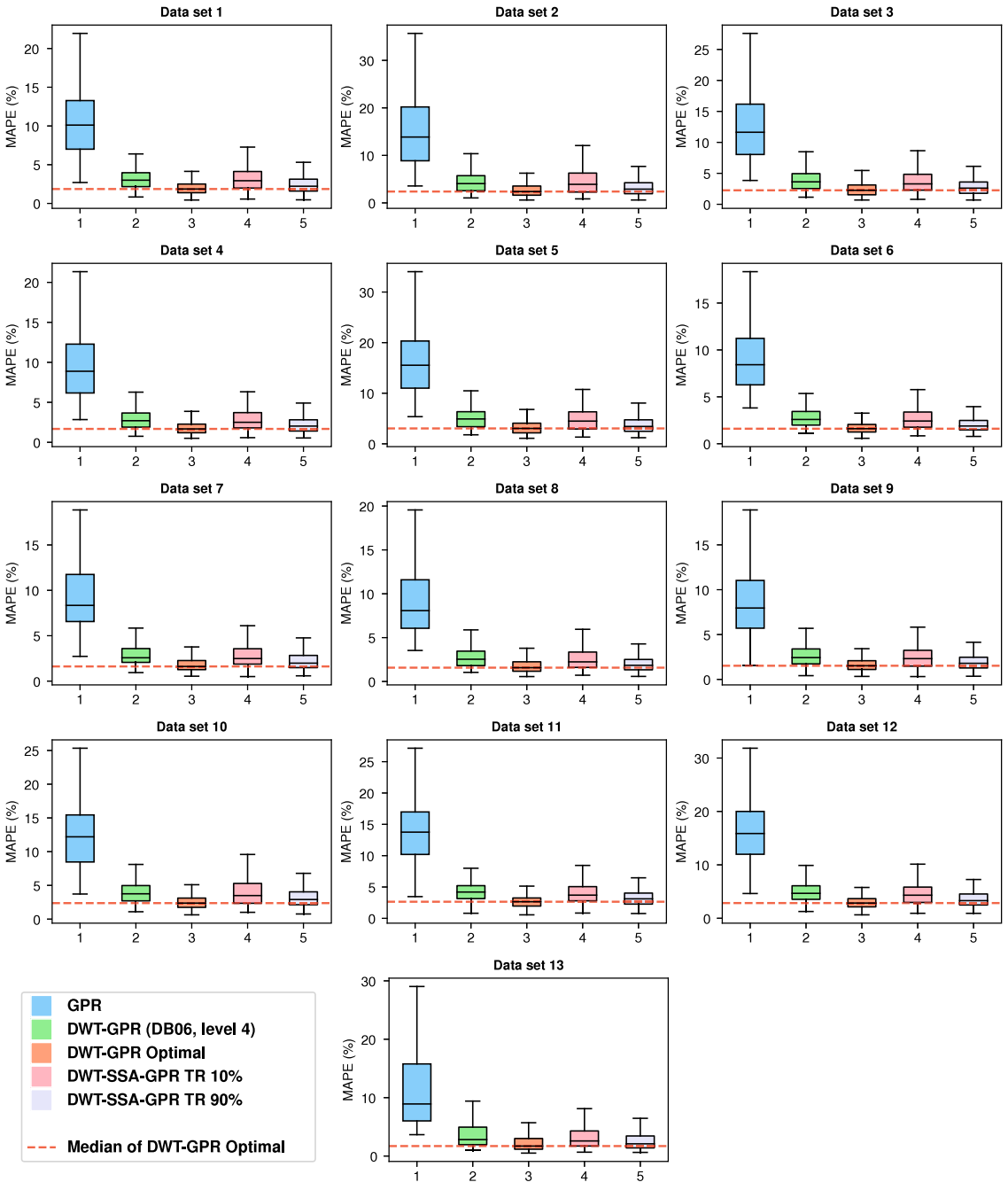

Fig. 5. MAPE for GPR prediction with different hyperparameters of data preprocessing techniques.

Table 4
Optimal Daubechies function order and decomposition level for each dataset.

Model	Optimal Daubechies function order												
	DS01	DS02	DS03	DS04	DS05	DS06	DS07	DS08	DS09	DS10	DS11	DS12	DS13
SVR	DB 10	DB 10	DB 19	DB 32	DB 32	DB 17	DB 26	DB 22	DB 23	DB 19	DB 16	DB 37	DB 32
GPR	DB 25	DB 32	DB 25	DB 32	DB 25	DB 32	DB 25	DB 25	DB 25	DB 25	DB 25	DB 32	DB 25
WNN	DB 16	DB 16	DB 19	DB 19	DB 19	DB 23	DB 16	DB 19	DB 19	DB 19	DB 19	DB 19	DB 19
LSTM	DB 37	DB 38	DB 37	DB 34	DB 38	DB 37	DB 32	DB 34	DB 38	DB 32	DB 30	DB 37	DB 34
Model	Optimal decomposition level												
	DS01	DS02	DS03	DS04	DS05	DS06	DS07	DS08	DS09	DS10	DS11	DS12	DS13
SVR	Level 4	Level 4	Level 2	Level 2	Level 3	Level 3	Level 2	Level 2	Level 3	Level 3	Level 4	Level 3	Level 2
GPR	Level 3	Level 4	Level 3	Level 4	Level 3	Level 4	Level 5	Level 4	Level 4	Level 5	Level 4	Level 4	Level 4
WNN	Level 3	Level 3	Level 3	Level 3	Level 3	Level 3	Level 4	Level 3	Level 3	Level 3	Level 3	Level 3	Level 3
LSTM	Level 4	Level 4	Level 4	Level 5	Level 4	Level 4	Level 5	Level 4	Level 4	Level 4	Level 3	Level 5	Level 5

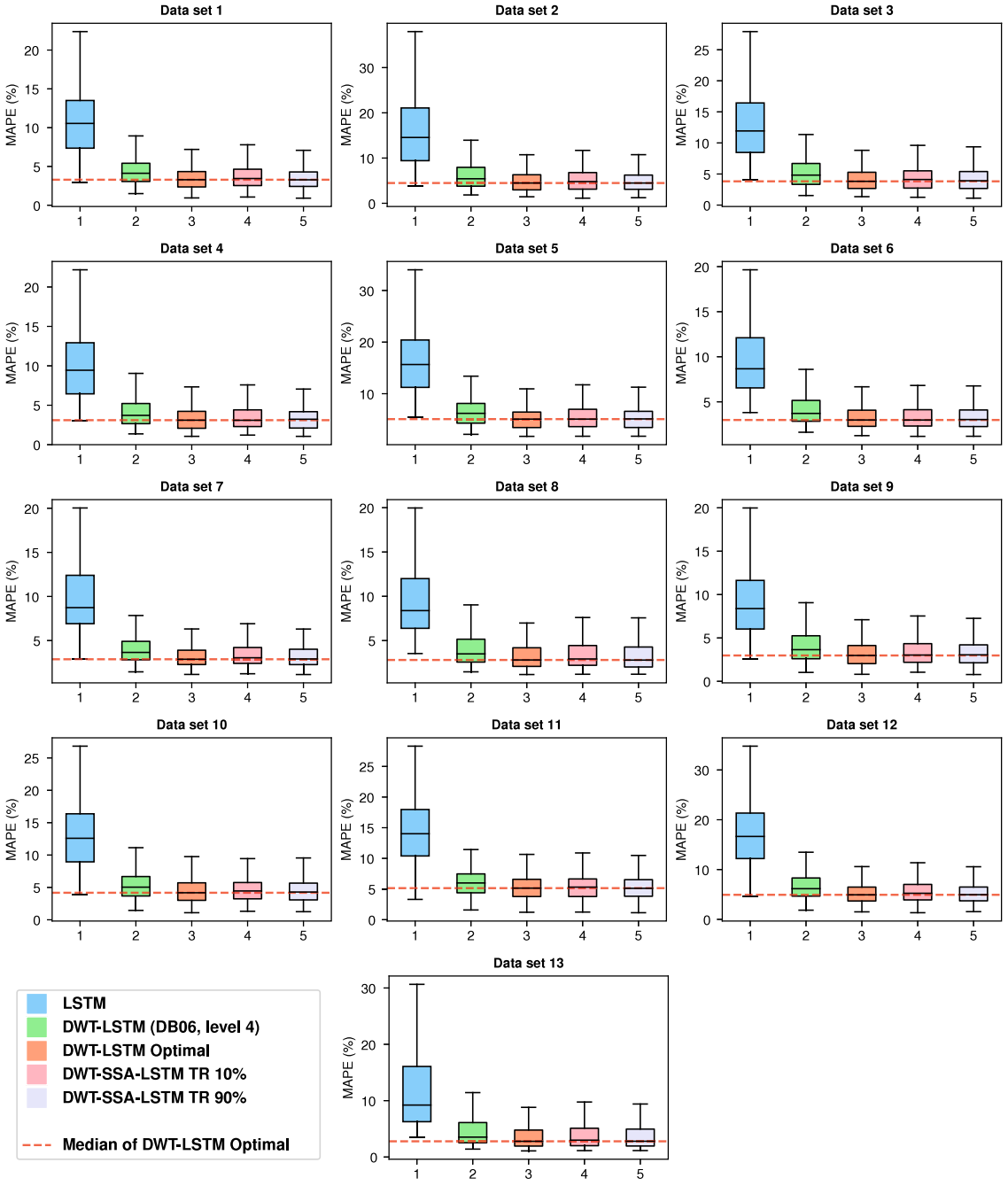

Fig. 6. MAPE for LSTM prediction with different hyperparameters of data preprocessing techniques.

coefficient (ρ).

$$\mathrm{MSE} = \frac{1}{T}\sum_{t=1}^{T}\left(y_{\mathrm{test}}(t) - y_{\mathrm{predict}}(t)\right)^2 \tag{7}$$

$$\mathrm{MAE} = \frac{1}{T}\sum_{t=1}^{T}\left|y_{\mathrm{test}}(t) - y_{\mathrm{predict}}(t)\right| \tag{8}$$

$$\mathrm{MAPE} = \frac{1}{T}\sum_{t=1}^{T}\frac{\left|y_{\mathrm{test}}(t) - y_{\mathrm{predict}}(t)\right|}{y_{\mathrm{test}}(t)} \times 100\% \tag{9}$$

$$\mathrm{MPE} = \frac{1}{T}\sum_{t=1}^{T}\frac{y_{\mathrm{test}}(t) - y_{\mathrm{predict}}(t)}{y_{\mathrm{test}}(t)} \times 100\% \tag{10}$$

$$R^2 = 1 - \frac{\sum_{t=1}^{T}\left(y_{\mathrm{predict}}(t) - y_{\mathrm{test}}(t)\right)^2}{\sum_{t=1}^{T}\left(y_{\mathrm{test}}(t) - \bar{y}_{\mathrm{test}}(t)\right)^2} \tag{11}$$

$$\rho = \frac{\mathrm{cov}\left(y_{\mathrm{test}}, y_{\mathrm{predict}}\right)}{\sigma_{y_{\mathrm{test}}}\,\sigma_{y_{\mathrm{predict}}}}. \tag{12}$$

where, y_{test} is the observed data, y_{predict} is the predicted data, and T is the length of data.

After using DWT with different decomposition levels and wavelet function orders, Table 4 shows the optimal order of the Daubechies wavelet function and the corresponding decomposition levels found for each of the examined datasets with different prediction models. The results reported here provide a general understanding of the effect of the Daubechies wavelet function order on the performance of various prediction models in the study. It has been demonstrated that the ideal order of the Daubechies function for DWT with SVR depends on the characteristics of the data and typically falls between 16 to 32. This is because higher-order wavelets can lead to overfitting and

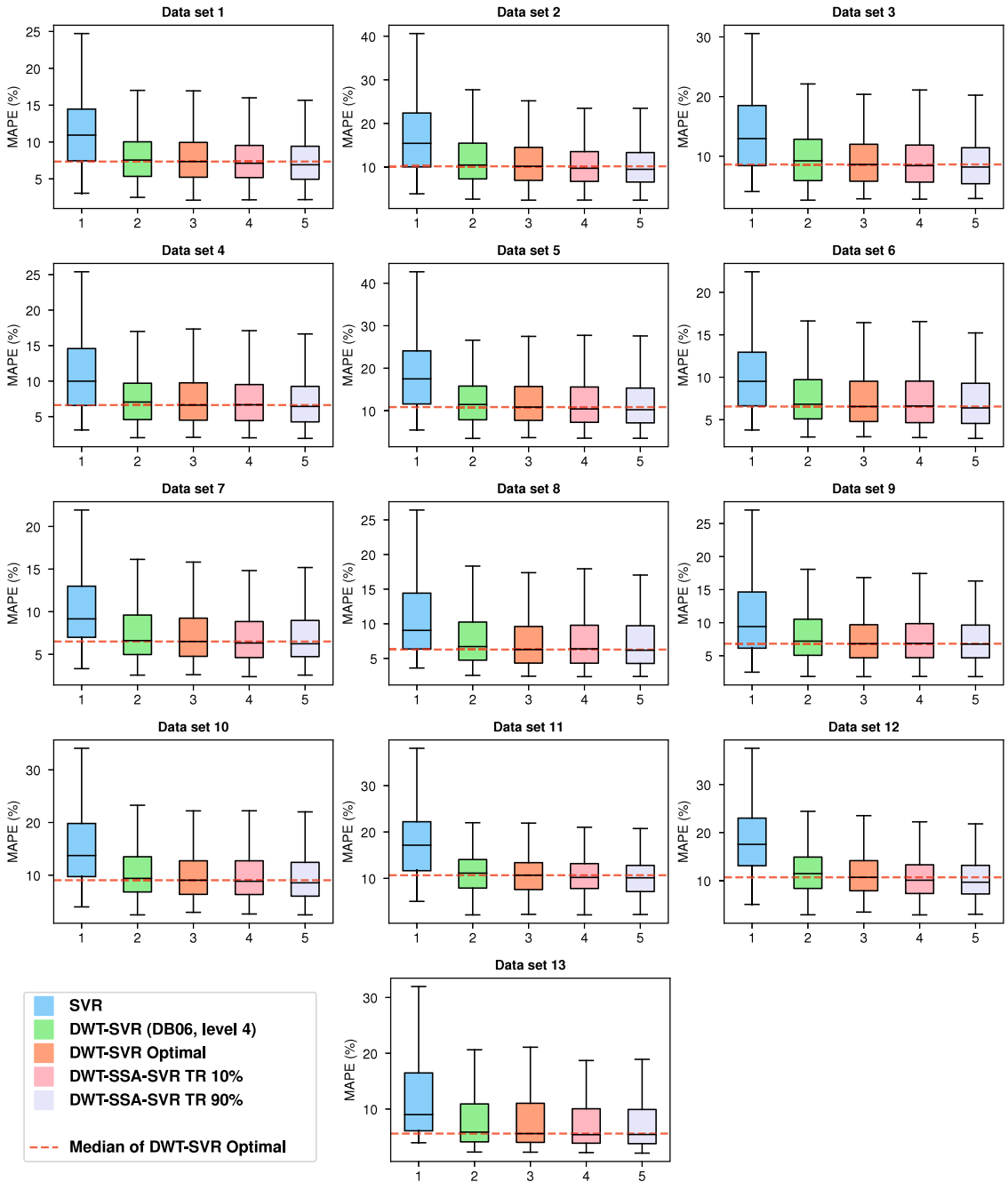

Fig. 7. MAPE for SVR prediction with different hyperparameters of data preprocessing techniques.

lower-order wavelets can lead to underfitting. When DWT is used with GPR, LSTM, or WNN, the optimal order of the Daubechies function is influenced by the prediction model used. Particularly, the results show that the ideal order for GPR across the majority of datasets is 25, whereas the optimal order for WNN is 19, and the optimal order for LSTM is relatively high, generally above 32. That means GPR as a probabilistic model that assumes a Gaussian distribution over the target variable, works better with a specific wavelet function order that can capture the smoothness of the signal. In contrast, LSTM as a type of recurrent neural network that can capture long-term temporal dependencies, benefits from a higher-order wavelet function that can capture more complex signal patterns. In general, higher-order wavelets may be more suitable for WNN. However, the choice of the Daubechies function order may also depend on the number of layers and neurons in the WNN architecture, as well as other hyperparameters such as the learning rate and regularization strength. Furthermore, the results suggest that the third and fourth decomposition levels are best for the majority of the datasets and various prediction models. However, using decomposition levels 2 and 5 results in improved performance for some datasets, particularly DS04, DS07, and DS13. Higher decomposition levels can capture more detailed and fine-grained variations in the wind speed time series, but can also be more susceptible to noise and overfitting. Lower decomposition levels, on the other hand, may provide a smoother representation of the signal but may miss important details and patterns.

The performance of the DWT model using optimal hyperparameters is illustrated in Figs. 5 and 6, showcasing the results for GPR and LSTM, respectively. The results, in terms of MAPE, are juxtaposed against the performance of the standalone prediction model, the DWT employing the Daubechies 6 (DB06) wavelet with level 4 decomposition, and the

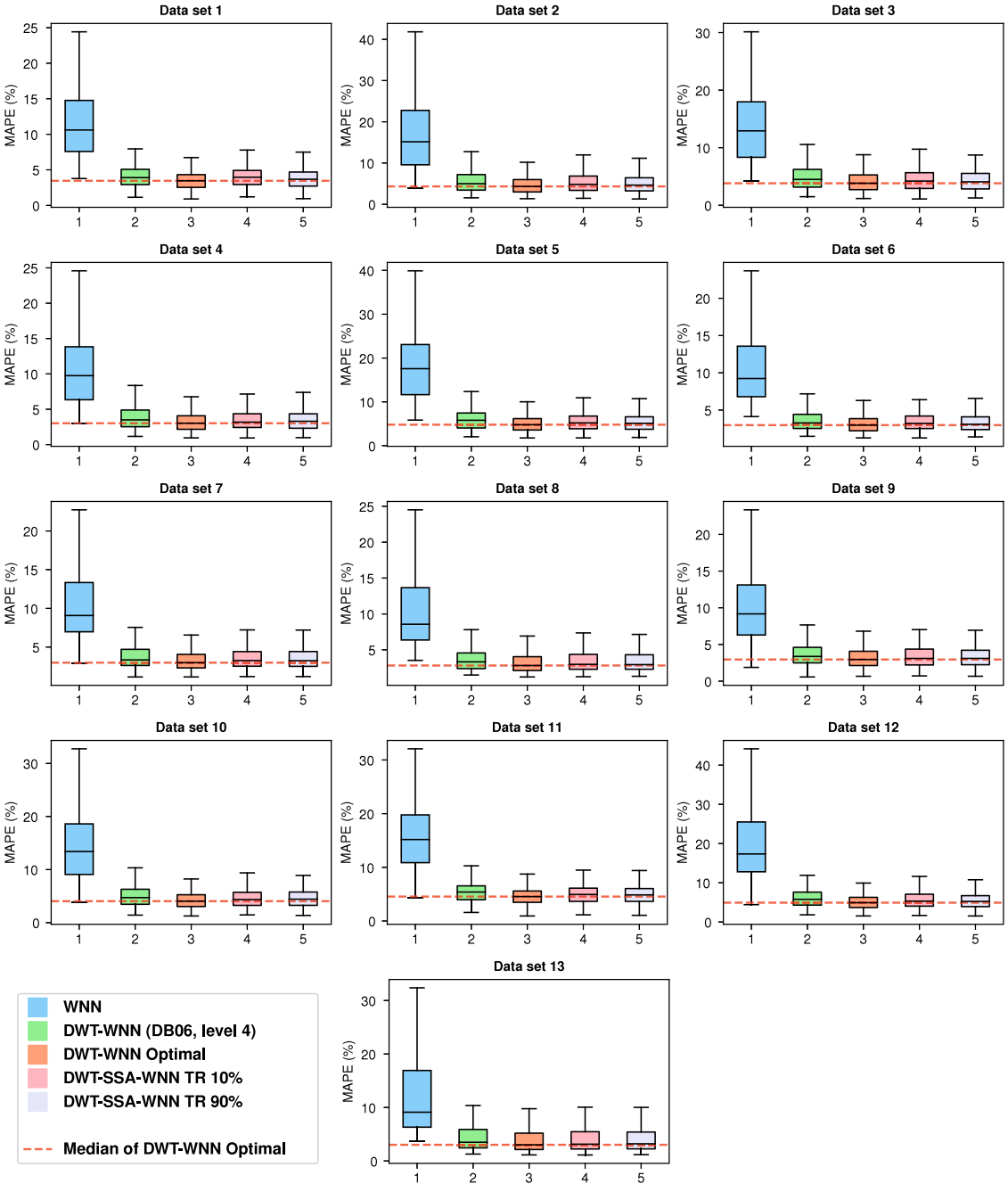

Fig. 8. MAPE for WNN prediction with different hyperparameters of data preprocessing techniques.

blend of DWT-SSA with TR equal to 10% and 90%. It's pertinent to highlight that the scales of the y-axis vary in each subplot to accentuate the distinctions among the various models. The data reveals that using optimal hyperparameters in the DWT model significantly enhances its efficacy compared to the DB06 wavelet at decomposition level 4. Among the combinations, DWT-SSA with a TR of 90% stands out as the most proficient compared to other TR values. The performance contrast is especially evident for the GPR and LSTM models, prompting their detailed presentation here. On the other hand, the SVR and WNN models exhibit less contrast in their performance and their detailed results are presented in Figs. 7 and 8. An exhaustive review of the performance metrics for all prediction models, assessed using diverse criteria, is available in Tables 6–9.

Table 10 shows the performance of various prediction models (SVR, GPR, WNN, and LSTM) compared across different scenarios, with the persistence model serving as a reference. The models' performances are evaluated under the following conditions: sole prediction, combined with DWT (DB06, level4), combined with DWT (optimal), and finally, combined with DWT-SSA (Optimal + TR=90%). The performance metrics used for comparison are MSE and MAPE, normalised to the persistence model performance. For the sole prediction scenario, the MSE values show that GPR performs better than the persistence model with a value of 97.9%. On the other hand, SVR, WNN, and LSTM exhibit higher MSE values at 107.0%, 140.4%, and 103.6%, respectively. In terms of MAPE, all models perform similarly to the persistence model, with values ranging from 99.7% for GPR to 110.4% for WNN. Upon incorporating DWT (DB06, level4) into the analysis, all four prediction models demonstrate considerable improvements in both MSE and MAPE relative to the persistence model. The DWT-GPR model outperforms the others, achieving the lowest MSE at 11.3%. The

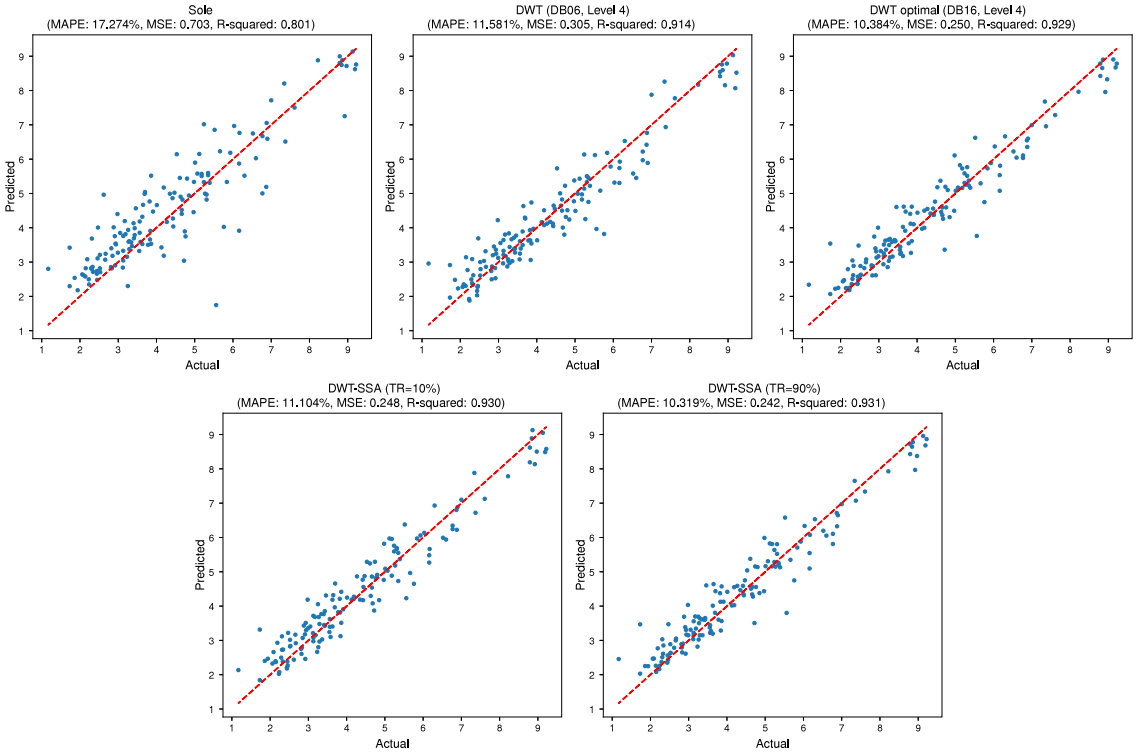

Fig. 9. Scatter plot: Actual vs. Predicted values from the SVR model using various data preprocessing hyperparameters.

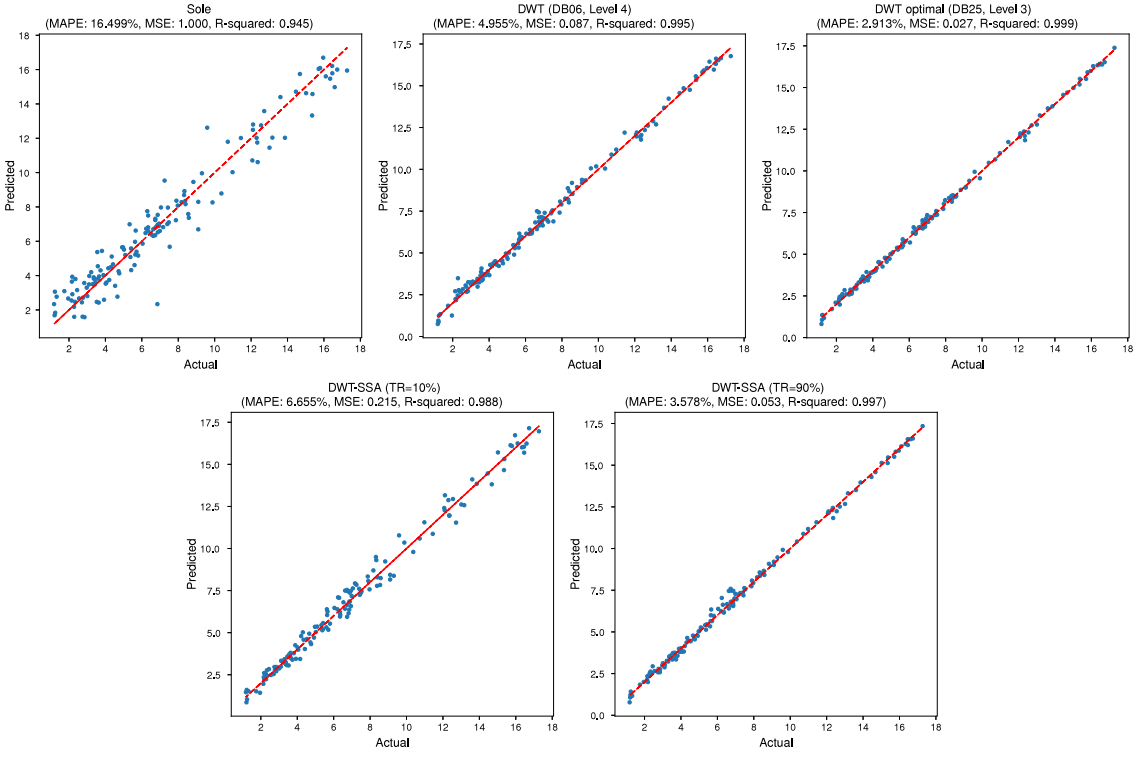

Fig. 10. Scatter plot: Actual vs. Predicted values from GPR model using various data preprocessing hyperparameters.

remaining models follow in this order: WNN at 15.6%, LSTM at 18.5%, and SVR at 52.7%. In terms of MAPE, the DWT-GPR model maintains its superior performance with the lowest value of 31.3%. The subsequent rankings are as follows: WNN with 39.7%, LSTM with 43.1%, and SVR with 76.4%. Furthermore, when the models are combined with DWT (optimal), further improvements in MSE and MAPE are observed compared to the persistence model. The DWT-GPR model achieves the lowest MSE of 5.2%, followed by WNN at 11.7%, LSTM at 11.9%, and SVR at 47.7%. In terms of MAPE, GPR maintains its leading position with a value of 19.5%, followed by WNN at 34.6%, LSTM at 34.9%, and

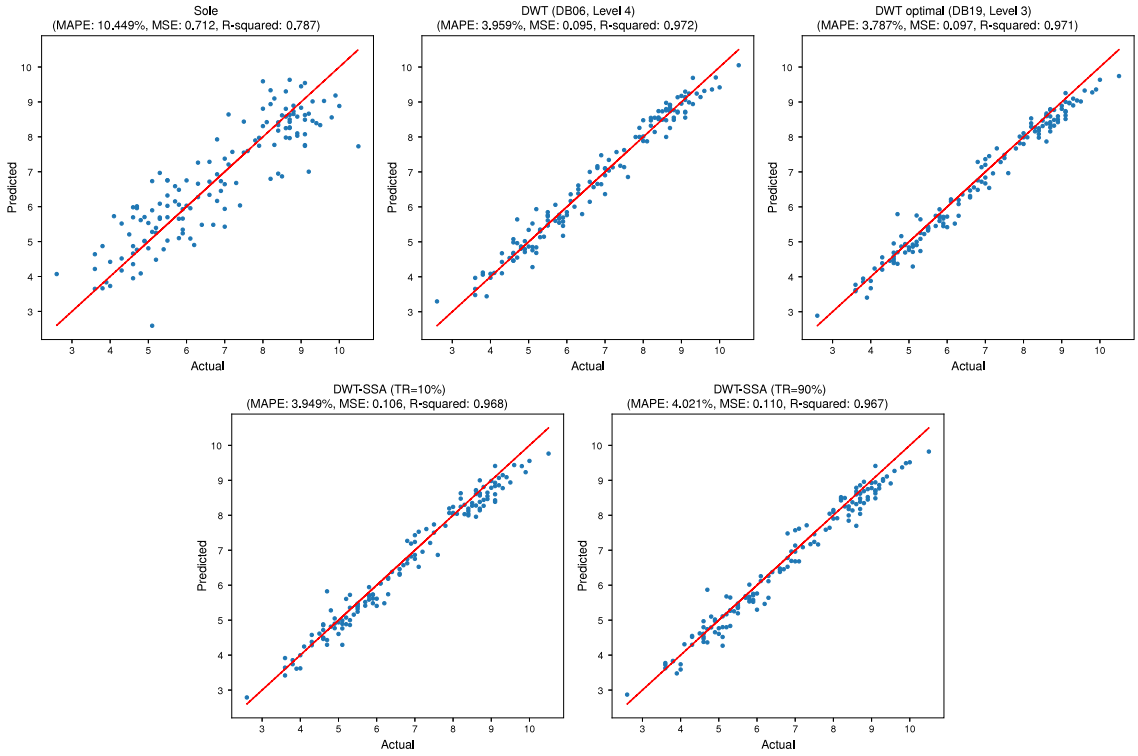

Fig. 11. Scatter plot: Actual vs. Predicted values from WNN model using various data preprocessing hyperparameters.

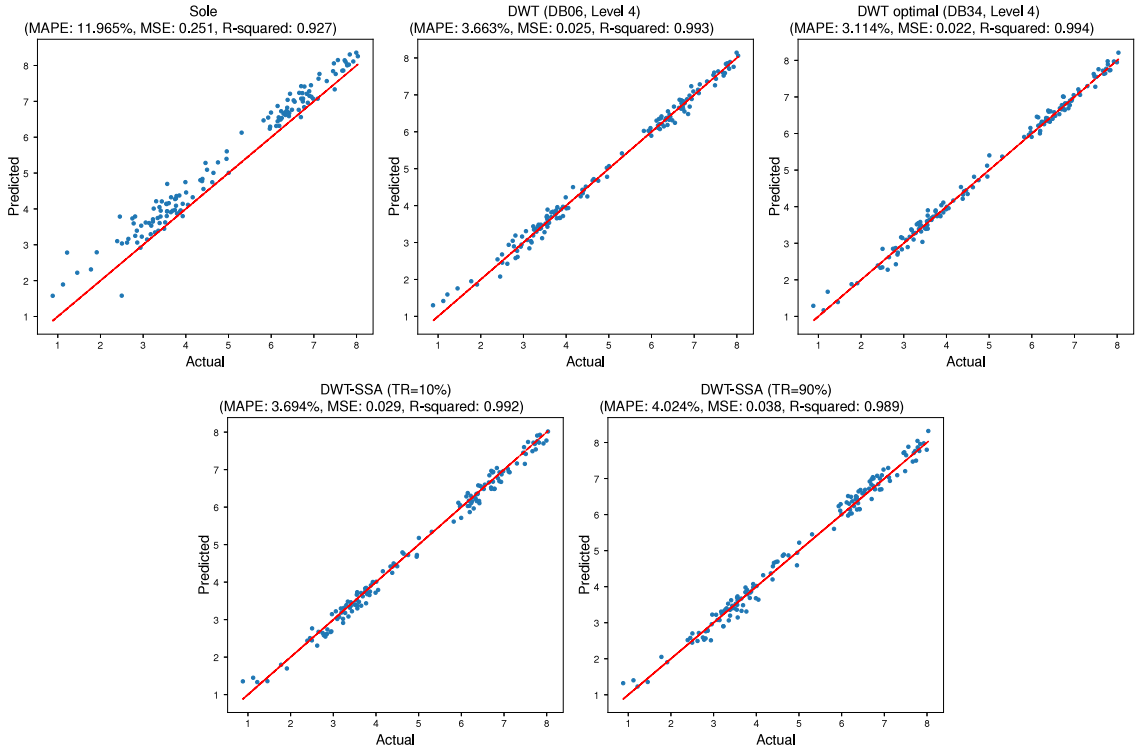

Fig. 12. Scatter plot: Actual vs. Predicted values from LSTM model using various data preprocessing hyperparameters.

SVR at 73.2%. Lastly, when the prediction models are combined with DWT-SSA (Optimal + TR=90%), the performance remains relatively consistent with the DWT (optimal) scenario. The DWT-SSA-GPR model achieves an MSE of 6.5%, while the other models show slight variations in their MSE and MAPE values. The DWT-SSA-SVR model exhibits the most significant improvement in MSE, with a value of 44.1% compared to the persistence model.

Our results are consistent with those in a previous study (Yu et al., 2017), which investigated the effectiveness of combining DWT with SSA under varying trend ratios, using DWT with DB06 and level 3.

Table 6
Error evaluation results of SVR over all datasets.

Model	Evaluation criteria	DS01	DS02	DS03	DS04	DS05	DS06	DS07	DS08	DS09	DS10	DS11	DS12	DS13
SVR	MSE (m/s)	0.6195	0.7982	0.5667	0.4226	0.4830	0.4811	0.4301	0.4525	0.4939	0.6141	0.7894	0.5968	0.4694
	MAE (m/s)	0.5721	0.6423	0.5495	0.4798	0.5192	0.5113	0.4861	0.4984	0.5142	0.5591	0.6410	0.5462	0.5042
	$MAPE$ (%)	11.5606	18.6355	14.4567	11.4775	18.9144	11.0560	10.6298	11.9636	12.8466	15.8782	17.4402	18.8160	13.0528
	MPE (%)	−4.7402	−10.8124	−7.1435	−5.7631	−10.7012	−5.4827	−4.2930	−6.6717	−7.9328	−9.2485	−10.3877	−10.1515	−5.4163
	R^2	0.8470	0.8399	0.8856	0.8772	0.8621	0.8837	0.8347	0.8812	0.8920	0.8702	0.8610	0.8550	0.8301
	ρ	0.9234	0.9242	0.9450	0.9423	0.9346	0.9468	0.9210	0.9455	0.9573	0.9411	0.9395	0.9278	0.9149
DWT-SVR (DB3, level 3)	MSE (m/s)	0.3149	0.4212	0.2700	0.2130	0.2340	0.2679	0.2334	0.2431	0.2835	0.3251	0.3929	0.2751	0.2105
	MAE (m/s)	0.4150	0.4775	0.3856	0.3433	0.3617	0.3813	0.3601	0.3636	0.3903	0.4132	0.4596	0.3790	0.3422
	$MAPE$ (%)	8.3250	13.6632	10.2882	8.0757	13.0671	8.1336	7.8138	8.2992	8.8494	11.5216	12.5292	12.8738	8.7197
	MPE (%)	−3.4728	−8.6422	−5.1262	−3.4874	−6.1071	−2.9806	−3.0861	−3.4616	−3.9945	−6.2671	−7.4058	−6.8592	−3.4431
	R^2	0.9221	0.9115	0.9442	0.9380	0.9323	0.9349	0.9093	0.9376	0.9387	0.9303	0.9278	0.9321	0.9225
	ρ	0.9634	0.9619	0.9746	0.9712	0.9685	0.9696	0.9576	0.9705	0.9725	0.9687	0.9708	0.9679	0.9624
DWT-SVR (DB4, level 3)	MSE (m/s)	0.3045	0.4004	0.2589	0.2081	0.2284	0.2605	0.2235	0.2302	0.2810	0.3080	0.3628	0.2680	0.2131
	MAE (m/s)	0.4084	0.4606	0.3787	0.3411	0.3585	0.3790	0.3521	0.3538	0.3893	0.4041	0.4348	0.3753	0.3450
	$MAPE$ (%)	8.1897	12.9951	10.0268	7.9612	13.1215	8.2515	7.6290	8.1224	8.9556	11.3320	11.7032	12.8336	8.8169
	MPE (%)	−3.3793	−7.6221	−4.7937	−3.2495	−6.5386	−3.6060	−2.5797	−3.4067	−4.2014	−6.6222	−6.3847	−6.6835	−3.4480
	R^2	0.9257	0.9172	0.9466	0.9389	0.9331	0.9345	0.9131	0.9403	0.9387	0.9344	0.9368	0.9327	0.9222
	ρ	0.9651	0.9642	0.9754	0.9720	0.9695	0.9704	0.9586	0.9721	0.9725	0.9715	0.9725	0.9685	0.9629
DWT-SVR (DB4, level 4)	MSE (m/s)	0.3083	0.3906	0.2701	0.2075	0.2250	0.2649	0.2281	0.2384	0.2941	0.3034	0.3694	0.2715	0.2099
	MAE (m/s)	0.4093	0.4531	0.3862	0.3369	0.3536	0.3815	0.3552	0.3593	0.3971	0.3979	0.4368	0.3762	0.3420
	$MAPE$ (%)	7.9971	12.2702	9.8448	7.6555	12.4793	8.0859	7.6076	8.1047	8.9628	10.8732	11.5817	12.3201	8.5770
	MPE (%)	−2.1705	**−5.3479**	**−3.6771**	**−2.3549**	**−4.8600**	**−2.6368**	**−2.3257**	**−2.8126**	−3.1006	−5.4219	−5.5782	−4.9124	−2.8516
	R^2	0.9247	0.9211	0.9448	0.9400	0.9354	0.9357	0.9125	0.9391	0.9378	0.9364	0.9357	0.9325	0.9235
	ρ	0.9634	0.9614	0.9738	0.9707	0.9690	0.9691	0.9574	0.9709	0.9701	0.9707	0.9712	0.9673	0.9626
DWT-SVR (DB6, level 4)	MSE (m/s)	0.3118	0.4002	0.2668	0.2050	0.2149	0.2622	0.2239	0.2565	0.2831	0.3026	0.3627	0.2676	0.2017
	MAE (m/s)	0.4163	0.4630	0.3836	0.3373	0.3492	0.3794	0.3543	0.3730	0.3908	0.3963	0.4354	0.3748	0.3352
	$MAPE$ (%)	8.1590	12.4499	9.9709	7.6535	12.3911	7.9754	7.5839	8.3230	8.6489	10.6833	11.3352	12.2317	8.4976
	MPE (%)	−2.4594	−5.6968	−3.7982	−2.2088	−4.9516	−2.5738	−2.3861	−2.9090	−2.7938	−4.9518	−4.6607	−4.8970	**−2.8400**
	R^2	0.9230	0.9173	0.9444	0.9404	0.9386	0.9372	0.9148	0.9357	0.9384	0.9367	0.9370	0.9339	0.9265
	ρ	0.9627	0.9603	0.9743	0.9711	0.9707	0.9696	0.9590	0.9698	0.9702	0.9709	0.9709	0.9681	0.9645
DWT-SVR Optimal	MSE (m/s)	0.2945	0.3538	0.2373	0.1902	0.1945	0.2348	0.2071	0.2200	0.2497	0.2760	0.3298	0.2453	0.1885
	MAE (m/s)	0.4038	0.4376	0.3652	0.3284	0.3335	0.3630	0.3437	0.3488	0.3663	0.3823	0.4152	0.3589	0.3280
	$MAPE$ (%)	7.9261	12.1642	9.5044	7.8174	11.9758	7.7340	7.4886	**7.9862**	8.0054	10.4215	10.7897	11.6154	8.2838
	MPE (%)	−2.0968	−5.6934	−4.4413	−3.3515	−5.6838	−2.8434	−2.9631	−3.5632	−2.6454	−4.4010	−4.5746	−4.1329	−3.1104
	R^2	0.9281	0.9271	0.9515	0.9439	0.9434	0.9418	0.9192	0.9432	0.9473	0.9394	0.9427	0.9395	0.9314
	ρ	0.9653	0.9651	0.9783	0.9747	0.9738	0.9728	0.9629	0.9744	0.9745	0.9724	0.9736	0.9706	0.9675
DWT-SSA-SVR TR 10%	MSE (m/s)	0.2820	0.3190	0.2303	0.1861	0.1854	0.2300	0.1986	0.2227	0.2545	0.2731	0.3285	0.2200	0.1710
	MAE (m/s)	0.3964	0.4139	0.3617	0.3258	0.3254	0.3605	0.3352	0.3507	0.3709	0.3807	0.4158	0.3403	0.3126
	$MAPE$ (%)	7.7625	11.4595	9.4368	7.7786	11.7599	7.6964	7.3120	8.0350	8.1042	10.3473	10.7182	10.9676	7.8347
	MPE (%)	−2.0299	−5.4237	−4.3929	−3.3177	−5.5989	−2.8267	−2.9401	−3.5452	−2.6303	−4.3150	**−4.4855**	−3.9299	−2.9757
	R^2	0.9316	0.9336	0.9518	0.9453	0.9461	0.9416	0.9227	0.9424	0.9461	0.9401	0.9429	0.9451	0.9369
	ρ	0.9672	0.9686	0.9785	0.9755	0.9752	0.9727	0.9648	0.9740	0.9739	0.9727	0.9737	0.9735	0.9704
DWT-SSA-SVR TR 70%	MSE (m/s)	0.2986	0.3457	0.2338	0.1940	0.1855	0.2346	0.2190	0.2265	0.2464	0.2894	0.3265	0.2317	0.1775
	MAE (m/s)	0.4069	0.4343	0.3649	0.3329	0.3257	0.3653	0.3546	0.3556	0.3638	0.3936	0.4148	0.3500	0.3186
	$MAPE$ (%)	7.9726	11.9856	9.5346	7.9426	11.7500	7.8195	7.6972	8.1709	7.9414	10.7698	10.7561	11.2460	8.0106
	MPE (%)	−2.0640	−5.5595	−4.3977	−3.3412	−5.6312	−2.8394	−2.9521	−3.5562	−2.6167	−4.3506	−4.5203	−3.9824	−3.0313
	R^2	0.9269	0.9276	0.9504	0.9425	0.9459	0.9406	0.9144	0.9409	0.9478	0.9349	0.9433	0.9422	0.9351
	ρ	0.9648	0.9655	0.9777	0.9739	0.9751	0.9722	0.9606	0.9732	0.9748	0.9703	0.9739	0.9720	0.9694
DWT-SSA-SVR TR 80%	MSE (m/s)	0.2877	0.3266	0.2257	0.1839	0.1822	0.2266	0.2090	0.2189	0.2469	0.2723	0.3152	0.2249	0.1735
	MAE (m/s)	0.3997	0.4205	0.3580	0.3232	0.3225	0.3578	0.3452	0.3490	0.3645	0.3788	0.4050	0.3453	0.3152
	$MAPE$ (%)	7.8264	11.6666	9.3568	7.7342	11.6601	7.6447	7.5013	8.0260	7.9415	10.3877	10.5124	11.0890	7.9042
	MPE (%)	−2.0473	−5.5137	−4.3757	−3.3282	−5.6101	−2.8323	−2.9415	−3.5501	−2.6129	−4.3330	−4.5086	−3.9328	−2.9873
	R^2	0.9307	0.9318	0.9524	0.9459	0.9468	0.9432	0.9188	0.9430	0.9476	0.9390	0.9454	0.9440	0.9363
	ρ	0.9667	0.9677	0.9788	0.9758	0.9756	0.9735	0.9627	0.9742	0.9747	0.9726	0.9750	0.9729	0.9701
DWT-SSA-SVR TR 90%	MSE (m/s)	**0.2675**	**0.3136**	**0.2163**	**0.1753**	**0.1751**	**0.2204**	**0.1971**	**0.2166**	**0.2446**	**0.2607**	**0.3093**	**0.2125**	**0.1667**
	MAE (m/s)	**0.3853**	**0.4112**	**0.3492**	**0.3151**	**0.3159**	**0.3519**	**0.3341**	**0.3471**	**0.3622**	**0.3693**	**0.4004**	**0.3344**	**0.3085**
	$MAPE$ (%)	**7.5419**	**11.4220**	**9.1456**	**7.5630**	**11.4715**	**7.5317**	**7.2893**	7.9998	**7.8920**	**10.0922**	**10.4116**	**10.7361**	**7.7575**
	MPE (%)	**−2.0219**	−5.4336	−4.3575	−3.3130	−5.5619	−2.8292	−2.9331	−3.5377	−2.6155	**−4.3027**	−4.4956	**−3.8556**	−2.9662
	R^2	**0.9358**	**0.9344**	**0.9551**	**0.9485**	**0.9489**	**0.9449**	**0.9233**	**0.9437**	**0.9482**	**0.9425**	**0.9466**	**0.9471**	**0.9389**
	ρ	**0.9694**	**0.9691**	**0.9802**	**0.9772**	**0.9767**	**0.9744**	**0.9651**	**0.9746**	**0.9749**	**0.9742**	**0.9756**	**0.9745**	**0.9715**

This study also found that a trend ratio of 90% (TR=90%) yields the best performance compared to other ratios. However, in our study, the combined approach of DWT with optimal hyperparameters and SSA using TR=90% does not outperform DWT alone. These findings suggest that the optimal hyperparameters of DWT lead to superior results compared to the DWT-SSA approach. This not only enhances the accuracy of forecasting but also reduces computational time.

The selection of a high-order or low-order Daubechies wavelet depends on the characteristics of the data being analysed. High-order wavelet functions can provide a more detailed visualisation of the frequency components in the signal, which can be useful for gaining insights into the underlying patterns and trends in the data. There may still be some level of noise presenting in the signal that could interfere with accurate wind speed predictions. A high-order wavelet function with multiple decomposition levels can be effective in removing noise from the signal and improving the accuracy of predictions. Additionally, the selection of the specific high-order Daubechies wavelet is influenced by the prediction model being used. Our findings suggest that different prediction models perform better with various high-order wavelets, and the exact order of the wavelet may need to be tuned based on the specific prediction model employed. The selection of the decomposition level of the Discrete Wavelet Transform lacks a specific rationale. It is worth observing that the decomposition level can vary for a given dataset when different prediction models are employed. Therefore, a consistent prediction model may require alterations to the decomposition level across various datasets. Moreover, the results show that combining the prediction models with DWT and DWT-SSA can significantly improve their performance compared to the persistence model. DWT (Optimal) scenario yields the best results, when combined with GPR, WNN, and LSTM. The SVR model performs better in DWT-SSA (Optimal + TR=90%) scenario compared to the other scenarios.

For our comparative analysis, we randomly select distinct datasets for each predictive model: Dataset 11 for SVR, Dataset 2 for GPR, Dataset 5 for WNN, and Dataset 9 for LSTM. This selection is done to present unbiased results across different models. As illustrated in Fig. 9, the scatter plots display the comparative performance of the SVR model under five different configurations: Sole, DWT (DB06 level 4),

Table 7
Error evaluation results of GPR over all datasets.

Model	Evaluation criteria	DS01	DS02	DS03	DS04	DS05	DS06	DS07	DS08	DS09	DS10	DS11	DS12	DS13
GPR	MSE (m/s)	0.5874	0.7325	0.5380	0.3906	0.4536	0.4319	0.3934	0.4003	0.3936	0.5515	0.7028	0.5740	0.4569
	MAE (m/s)	0.5433	0.5948	0.5241	0.4459	0.4923	0.4717	0.4544	0.4532	0.4361	0.5056	0.5702	0.5237	0.4922
	$MAPE$ (%)	10.3613	16.0520	12.6155	9.6883	15.9694	9.2431	9.4886	9.3880	9.0234	12.7614	13.7725	16.4774	12.1291
	MPE (%)	−2.3035	−6.1862	−3.4003	−1.9978	−5.1888	−1.8321	−1.9911	−2.0110	−1.9444	−3.6135	−3.8510	−5.8226	−3.9017
	R^2	0.8534	0.8556	0.8930	0.8880	0.8729	0.8986	0.8495	0.8951	0.9188	0.8853	0.8809	0.8605	0.8344
	ρ	0.9244	0.9259	0.9458	0.9431	0.9352	0.9487	0.9233	0.9469	0.9592	0.9419	0.9399	0.9286	0.9154
DWT-GPR (DB3, level 3)	MSE (m/s)	0.1030	0.1286	0.0926	0.0676	0.0817	0.0769	0.0728	0.0711	0.0694	0.1056	0.1274	0.0995	0.0819
	MAE (m/s)	0.2218	0.2421	0.2142	0.1818	0.2033	0.1930	0.1890	0.1860	0.1781	0.2122	0.2353	0.2154	0.2040
	$MAPE$ (%)	4.2109	6.3909	5.2236	3.9705	6.7421	3.7807	3.9286	3.8580	3.7996	5.3253	5.6675	6.7912	4.9992
	MPE (%)	−0.4109	−1.2517	−0.6083	−0.3361	−0.8862	−0.2924	−0.3239	−0.3524	−0.3603	−0.6895	−0.6507	−0.9787	−0.7196
	R^2	0.9739	0.9747	0.9814	0.9804	0.9769	0.9820	0.9719	0.9812	0.9855	0.9782	0.9789	0.9755	0.9698
	ρ	0.9869	0.9873	0.9907	0.9902	0.9884	0.9910	0.9859	0.9906	0.9928	0.9891	0.9894	0.9877	0.9848
DWT-GPR (DB4, level 3)	MSE (m/s)	0.0825	0.1018	0.0760	0.0536	0.0644	0.0596	0.0592	0.0553	0.0553	0.0896	0.1017	0.0789	0.0654
	MAE (m/s)	0.1952	0.2123	0.1891	0.1589	0.1779	0.1671	0.1659	0.1610	0.1551	0.1883	0.2067	0.1885	0.1793
	$MAPE$ (%)	3.7103	5.6411	4.5659	3.4664	5.8570	3.2570	3.4186	3.3383	3.2655	4.6648	4.9373	5.8572	4.2864
	MPE (%)	−0.3290	−1.0047	−0.4240	−0.2584	−0.6313	−0.2091	−0.2476	−0.2731	−0.3075	−0.5310	−0.4557	−0.7486	−0.5097
	R^2	0.9795	0.9802	0.9848	0.9844	0.9818	0.9860	0.9773	0.9853	0.9884	0.9814	0.9830	0.9806	0.9757
	ρ	0.9897	0.9901	0.9924	0.9922	0.9909	0.9930	0.9887	0.9926	0.9942	0.9908	0.9915	0.9903	0.9878
DWT-GPR (DB4, level 4)	MSE (m/s)	0.0836	0.1039	0.0783	0.0543	0.0652	0.0603	0.0602	0.0556	0.0553	0.0947	0.1043	0.0794	0.0681
	MAE (m/s)	0.1961	0.2132	0.1903	0.1595	0.1786	0.1679	0.1669	0.1618	0.1556	0.1899	0.2079	0.1892	0.1810
	$MAPE$ (%)	3.7245	5.6703	4.5908	3.4805	5.8851	3.2759	3.4386	3.3583	3.2835	4.6998	4.9648	5.8749	4.3238
	MPE (%)	−0.3449	−1.0565	−0.4425	−0.2672	−0.6244	−0.2278	−0.2796	−0.2748	−0.2857	−0.5471	−0.4652	−0.7950	−0.5460
	R^2	0.9791	0.9798	0.9845	0.9841	0.9816	0.9858	0.9770	0.9851	0.9884	0.9802	0.9829	0.9804	0.9744
	ρ	0.9895	0.9899	0.9923	0.9921	0.9908	0.9929	0.9885	0.9926	0.9942	0.9903	0.9915	0.9902	0.9873
DWT-GPR (DB6, level 4)	MSE (m/s)	0.0642	0.0824	0.0629	0.0412	0.0511	0.0476	0.0485	0.0433	0.0447	0.0806	0.0821	0.0582	0.0562
	MAE (m/s)	0.1687	0.1842	0.1656	0.1370	0.1536	0.1455	0.1443	0.1404	0.1349	0.1671	0.1808	0.1616	0.1580
	$MAPE$ (%)	3.1756	4.6657	3.9184	2.9675	5.0933	2.8420	2.9111	2.8935	2.8572	4.0888	4.2949	4.8982	3.6816
	MPE (%)	−0.2099	−0.6765	−0.3149	−0.1740	−0.3875	−0.1411	−0.1675	−0.1966	−0.1890	−0.3754	−0.3160	−0.5452	−0.3630
	R^2	0.9838	0.9842	0.9876	0.9881	0.9858	0.9887	0.9814	0.9885	0.9905	0.9826	0.9863	0.9855	0.9781
	ρ	0.9920	0.9921	0.9939	0.9941	0.9929	0.9944	0.9908	0.9943	0.9953	0.9917	0.9932	0.9928	0.9892
DWT-GPR Optimal	MSE (m/s)	**0.0297**	**0.0347**	**0.0280**	**0.0184**	**0.0238**	**0.0212**	**0.0218**	**0.0206**	**0.0202**	**0.0407**	**0.0392**	**0.0255**	**0.0241**
	MAE (m/s)	**0.1073**	**0.1137**	**0.1031**	**0.0842**	**0.0960**	**0.0891**	**0.0905**	**0.0879**	**0.0843**	**0.1067**	**0.1148**	**0.0997**	**0.0980**
	$MAPE$ (%)	**2.0168**	**2.8488**	**2.4483**	**1.8264**	**3.2271**	**1.7671**	**1.8419**	**1.8308**	**1.7587**	**2.6172**	**2.7451**	**3.0444**	**2.3178**
	MPE (%)	**−0.0686**	**−0.2552**	**−0.0822**	**−0.0379**	**−0.0848**	**−0.0189**	**−0.0612**	**−0.0534**	**−0.0659**	**−0.1383**	**−0.0977**	**−0.1404**	**−0.1454**
	R^2	**0.9925**	**0.9935**	**0.9945**	**0.9944**	**0.9936**	**0.9946**	**0.9915**	**0.9946**	**0.9957**	**0.9917**	**0.9935**	**0.9936**	**0.9908**
	ρ	**0.9963**	**0.9968**	**0.9973**	**0.9972**	**0.9968**	**0.9974**	**0.9958**	**0.9973**	**0.9979**	**0.9961**	**0.9968**	**0.9968**	**0.9954**
DWT-SSA-GPR TR 10%	MSE (m/s)	0.0774	0.0880	0.0612	0.0452	0.0495	0.0512	0.0480	0.0433	0.0424	0.0716	0.0763	0.0679	0.0537
	MAE (m/s)	0.1799	0.1919	0.1652	0.1386	0.1520	0.1472	0.1456	0.1352	0.1307	0.1620	0.1750	0.1665	0.1527
	$MAPE$ (%)	3.3791	4.7266	3.9368	2.9423	4.9542	2.8066	2.9924	2.7914	2.6950	4.0552	4.1507	5.0685	3.5212
	MPE (%)	−0.1034	−0.2972	−0.1381	−0.0615	−0.1090	−0.0407	−0.0866	−0.0863	−0.0969	−0.2228	−0.1436	−0.2460	−0.2252
	R^2	0.9795	0.9823	0.9874	0.9842	0.9853	0.9859	0.9812	0.9879	0.9914	0.9850	0.9871	0.9829	0.9793
	ρ	0.9900	0.9914	0.9938	0.9924	0.9928	0.9932	0.9908	0.9940	0.9958	0.9927	0.9936	0.9916	0.9899
DWT-SSA-GPR TR 70%	MSE (m/s)	0.0672	0.0628	0.0489	0.0350	0.0384	0.0354	0.0411	0.0326	0.0333	0.0663	0.0622	0.0511	0.0434
	MAE (m/s)	0.1693	0.1674	0.1496	0.1276	0.1340	0.1270	0.1364	0.1226	0.1187	0.1615	0.1611	0.1516	0.1422
	$MAPE$ (%)	3.1535	4.1530	3.5287	2.7691	4.3606	2.4494	2.8252	2.5560	2.4500	4.0018	3.8709	4.5789	3.3197
	MPE (%)	−0.1142	−0.2628	−0.0875	−0.0556	−0.1039	−0.0302	−0.0853	−0.0741	−0.0813	−0.1763	−0.1320	−0.2005	−0.1756
	R^2	0.9827	0.9875	0.9901	0.9889	0.9894	0.9910	0.9838	0.9910	0.9932	0.9858	0.9893	0.9871	0.9830
	ρ	0.9915	0.9938	0.9951	0.9945	0.9948	0.9956	0.9920	0.9955	0.9966	0.9931	0.9947	0.9937	0.9916
DWT-SSA-GPR TR 80%	MSE (m/s)	0.0481	0.0509	0.0420	0.0279	0.0330	0.0304	0.0330	0.0285	0.0278	0.0567	0.0532	0.0399	0.0380
	MAE (m/s)	0.1458	0.1489	0.1346	0.1125	0.1213	0.1157	0.1215	0.1122	0.1073	0.1451	0.1478	0.1328	0.1291
	$MAPE$ (%)	2.7503	3.6955	3.1981	2.4663	3.9855	2.2547	2.5083	2.3444	2.2466	3.5786	3.5887	4.0577	2.9934
	MPE (%)	−0.0948	−0.2597	−0.1081	−0.0515	−0.1187	−0.0309	−0.0758	−0.0654	−0.0773	−0.1691	−0.1271	−0.1912	−0.1605
	R^2	0.9876	0.9902	0.9920	0.9914	0.9909	0.9923	0.9870	0.9923	0.9941	0.9882	0.9907	0.9901	0.9861
	ρ	0.9939	0.9951	0.9960	0.9958	0.9955	0.9962	0.9935	0.9962	0.9971	0.9943	0.9954	0.9951	0.9931
DWT-SSA-GPR TR 90%	MSE (m/s)	0.0397	0.0452	0.0345	0.0238	0.0292	0.0276	0.0284	0.0253	0.0244	0.0498	0.0487	0.0327	0.0316
	MAE (m/s)	0.1309	0.1371	0.1213	0.1019	0.1126	0.1070	0.1098	0.1030	0.0982	0.1313	0.1366	0.1191	0.1187
	$MAPE$ (%)	2.4666	3.4737	2.8752	2.2219	3.7551	2.0824	2.2457	2.1458	2.0477	3.2752	3.2731	3.6520	2.8048
	MPE (%)	−0.0870	−0.3504	−0.1069	−0.0529	−0.1079	−0.0308	−0.0773	−0.0650	−0.0874	−0.1718	−0.1275	−0.1846	−0.2013
	R^2	0.9898	0.9914	0.9932	0.9926	0.9919	0.9931	0.9887	0.9934	0.9948	0.9899	0.9918	0.9919	0.9882
	ρ	0.9950	0.9957	0.9966	0.9964	0.9960	0.9966	0.9944	0.9967	0.9974	0.9951	0.9959	0.9960	0.9941

DWT optimal, DWT-SSA TR=10%, and DWT-SSA TR=90%. The x-axis consistently represents the observed values, while the y-axis denotes the predicted values by the SVR model under each configuration. Notably, the DWT optimal configuration significantly outperforms the DWT (DB06 level 4), showcasing its superior predictive capability. Additionally, the DWT-SSA TR=90% configuration emerges as the most superior for the SVR model, indicating its enhanced capability in capturing the underlying patterns of the dataset.

Regarding Fig. 10, the scatter plots present the performance comparison of the GPR model under the same five configurations mentioned earlier. The efficacy of each configuration in fine-tuning the GPR model's prediction accuracy can be visually gauged. Among these configurations, the DWT optimal case seems especially prominent in its prediction accuracy. In Fig. 11, the scatter plots delineate the performance of the WNN model under these configurations. The distribution of points in each plot offers insights into how each configuration affects the WNN model's forecast accuracy, with the tight clustering for DWT optimal case. Lastly, Fig. 12 portrays the LSTM model's predictive performance under the same configurations. Given the LSTM model's inherent capability to handle long-term dependencies, configurations like the DWT optimal case might amplify its predictive skill, as evident from the clustering of data points around the line of perfect prediction.

5. Discussion

The nuanced relationship between the optimal order of the Daubechies wavelet function and the prediction model used underscores the intricate interplay between the characteristics of datasets and the architecture of models. In the case of SVR, the results point towards a sweet spot for the Daubechies function order, typically lying between 16 and 32. This range indicates a balance to prevent overfitting seen with higher-order wavelets and the underfitting associated with lower orders. The data's inherent characteristics and the model's structure inherently influence this balance. For example, the GPR, which inherently assumes a Gaussian distribution over the target variable, matches a wavelet function order that can mirror the inherent smoothness of the signal. Conversely, the LSTM, built to identify long-term temporal dependencies, aligns with a higher-order Daubechies function, catering to more intricate signal patterns.

Moreover, our analysis surrounding decomposition levels indicates that the optimal level is not universal, but rather, contingent on the specifics of the dataset and the prediction model. Higher decomposition levels delve deeper into the intricacies of the wind speed time series. However, with such granularity comes susceptibility to noise and the

Table 8
Error evaluation results of WNN over all datasets.

Model	Evaluation criteria	DS01	DS02	DS03	DS04	DS05	DS06	DS07	DS08	DS09	DS10	DS11	DS12	DS13
WNN	MSE (m/s)	0.6955	1.0699	0.7303	0.4532	0.6068	0.5802	0.6226	0.5453	0.7339	1.0016	1.0996	0.7904	0.5448
	MAE (m/s)	0.5950	0.6552	0.5697	0.4774	0.5369	0.5276	0.5122	0.4988	0.5200	0.5725	0.6464	0.5726	0.5247
	$MAPE$ (%)	12.4193	19.4683	14.7763	11.2166	18.9019	11.5044	11.4266	11.4908	12.3080	15.6783	16.3233	19.6710	14.8961
	MPE (%)	−4.5060	−9.7679	−5.8521	−3.6865	−8.1779	−4.0797	−3.8648	−4.1711	−5.1297	−6.3842	−6.4467	−9.0338	−6.7589
	R^2	0.8308	0.8047	0.8727	0.8759	0.8512	0.8737	0.8220	0.8746	0.8574	0.8531	0.8409	0.8337	0.8102
	ρ	0.9194	0.9161	0.9391	0.9388	0.9263	0.9413	0.9147	0.9393	0.9444	0.9287	0.9265	0.9172	0.9076
DWT-WNN	MSE (m/s)	0.1275	0.1537	0.1108	0.0812	0.0944	0.0989	0.0899	0.0910	0.0949	0.1251	0.1540	0.1124	0.0964
(DB3, level 3)	MAE (m/s)	0.2526	0.2687	0.2365	0.2023	0.2197	0.2217	0.2150	0.2144	0.2128	0.2364	0.2627	0.2322	0.2238
	$MAPE$ (%)	4.7907	6.7122	5.7953	4.4400	7.2915	4.3974	4.4786	4.5117	4.4369	5.9667	6.3661	7.3665	5.3189
	MPE (%)	−0.6664	−1.7136	−1.0976	−0.6575	−1.4512	−0.7034	−0.6120	−0.7800	−0.7982	−0.9824	−1.2607	−1.5809	−0.9365
	R^2	0.9682	0.9696	0.9778	0.9767	0.9735	0.9769	0.9657	0.9763	0.9805	0.9740	0.9747	0.9723	0.9645
	ρ	0.9843	0.9849	0.9890	0.9885	0.9868	0.9887	0.9831	0.9884	0.9905	0.9871	0.9875	0.9862	0.9824
DWT-WNN	MSE (m/s)	0.1127	0.1310	0.0935	0.0708	0.0796	0.0831	0.0775	0.0794	0.0870	0.1086	0.1327	0.0951	0.0807
(DB4, level 3)	MAE (m/s)	0.2316	0.2425	0.2129	0.1841	0.1956	0.1980	0.1951	0.1948	0.2000	0.2159	0.2376	0.2074	0.2005
	$MAPE$ (%)	4.3641	6.0116	5.1226	4.0227	6.4545	3.8984	4.0257	4.0642	4.1314	5.3724	5.7418	6.4469	4.6719
	MPE (%)	−0.6059	−1.5252	−0.9486	−0.5863	−1.2610	−0.6072	−0.6153	−0.6794	−0.7066	−0.8930	−1.1903	−1.3997	−0.8032
	R^2	0.9719	0.9740	0.9812	0.9796	0.9778	0.9804	0.9710	0.9793	0.9820	0.9777	0.9782	0.9765	0.9701
	ρ	0.9863	0.9872	0.9907	0.9901	0.9890	0.9904	0.9859	0.9900	0.9914	0.9890	0.9893	0.9884	0.9854
DWT-WNN	MSE (m/s)	0.1078	0.1301	0.0965	0.0696	0.0801	0.0839	0.0757	0.0805	0.0853	0.1080	0.1319	0.0961	0.0793
(DB4, level 4)	MAE (m/s)	0.2247	0.2423	0.2158	0.1825	0.1970	0.1992	0.1918	0.1960	0.1960	0.2159	0.2363	0.2084	0.1991
	$MAPE$ (%)	4.2515	5.9845	5.1816	3.9814	6.4861	3.9074	3.9471	4.0718	4.0431	5.3959	5.6807	6.4655	4.6216
	MPE (%)	−0.5476	−1.3957	−0.8163	−0.4746	−1.1387	−0.4544	−0.5335	−0.5465	−0.6454	−0.9635	−0.9743	−1.2487	−0.7313
	R^2	0.9732	0.9741	0.9805	0.9799	0.9776	0.9802	0.9715	0.9790	0.9824	0.9777	0.9785	0.9763	0.9705
	ρ	0.9869	0.9872	0.9905	0.9902	0.9889	0.9904	0.9862	0.9898	0.9916	0.9891	0.9894	0.9883	0.9858
DWT-WNN	MSE (m/s)	0.0950	0.1099	0.0814	0.0623	0.0639	0.0713	0.0656	0.0680	0.0736	0.0953	0.1099	0.0835	0.0707
(DB6, level 4)	MAE (m/s)	0.2193	0.2306	0.2043	0.1788	0.1836	0.1881	0.1840	0.1852	0.1881	0.2078	0.2271	0.2003	0.1936
	$MAPE$ (%)	4.0846	5.5926	4.8560	3.8667	5.9887	3.6596	3.7517	3.8164	3.8123	5.1182	5.4057	6.1034	4.4665
	MPE (%)	**−0.4741**	−1.1056	−0.6892	**−0.3955**	−0.8825	**−0.3806**	**−0.4878**	**−0.4631**	**−0.4626**	−0.7226	**−0.8306**	−1.0562	−0.6982
	R^2	0.9761	0.9782	0.9836	0.9819	0.9820	0.9835	0.9754	0.9824	0.9847	0.9804	0.9817	0.9796	0.9738
	ρ	0.9886	0.9894	0.9922	0.9914	0.9912	0.9921	0.9883	0.9917	0.9928	0.9906	0.9912	0.9901	0.9878
DWT-WNN	MSE (m/s)	**0.0702**	**0.0830**	**0.0609**	**0.0443**	**0.0484**	**0.0571**	**0.0519**	**0.0510**	**0.0566**	**0.0710**	**0.0842**	**0.0583**	**0.0528**
Optimal	MAE (m/s)	**0.1910**	**0.2012**	**0.1783**	**0.1523**	**0.1579**	**0.1688**	**0.1641**	**0.1612**	**0.1651**	**0.1804**	**0.1970**	**0.1698**	**0.1694**
	$MAPE$ (%)	**3.5626**	**4.7759**	**4.1393**	**3.2587**	**5.0753**	**3.2609**	**3.3176**	**3.3014**	**3.3115**	**4.3717**	**4.6196**	**5.1795**	**3.8034**
	MPE (%)	−0.5548	**−1.0747**	**−0.6751**	−0.4312	**−0.7404**	−0.4419	−0.5054	−0.5549	−0.5574	**−0.5382**	−0.9215	**−0.9405**	**−0.5298**
	R^2	**0.9824**	**0.9837**	**0.9876**	**0.9871**	**0.9865**	**0.9868**	**0.9809**	**0.9868**	**0.9882**	**0.9855**	**0.9865**	**0.9857**	**0.9802**
	ρ	**0.9922**	**0.9926**	**0.9947**	**0.9943**	**0.9938**	**0.9943**	**0.9915**	**0.9943**	**0.9950**	**0.9936**	**0.9939**	**0.9934**	**0.9917**
DWT-SSA-WNN	MSE (m/s)	0.0897	0.1018	0.0710	0.0519	0.0572	0.0669	0.0613	0.0593	0.0704	0.0809	0.0966	0.0718	0.0613
TR 10%	MAE (m/s)	0.2179	0.2236	0.1929	0.1646	0.1721	0.1827	0.1796	0.1738	0.1855	0.1938	0.2125	0.1881	0.1825
	$MAPE$ (%)	4.0498	5.3631	4.4849	3.5242	5.5197	3.5037	3.6326	3.5493	3.5980	4.7199	5.0058	5.7339	4.1054
	MPE (%)	−0.6014	−1.2043	−0.7096	−0.4647	−0.8227	−0.4538	−0.5468	−0.5910	−0.6310	−0.5892	−0.9747	−1.0250	−0.5854
	R^2	0.9774	0.9797	0.9857	0.9847	0.9840	0.9846	0.9772	0.9846	0.9858	0.9833	0.9841	0.9824	0.9770
	ρ	0.9897	0.9905	0.9937	0.9930	0.9926	0.9934	0.9897	0.9932	0.9940	0.9926	0.9927	0.9918	0.9902
DWT-SSA-WNN	MSE (m/s)	0.0954	0.1131	0.0812	0.0600	0.0646	0.0719	0.0598	0.0636	0.0976	0.0930	0.1093	0.0837	0.0713
TR 70%	MAE (m/s)	0.2210	0.2358	0.2065	0.1766	0.1838	0.1897	0.1773	0.1810	0.2204	0.2098	0.2280	0.2021	0.1971
	$MAPE$ (%)	4.1278	5.7076	4.7917	3.7866	5.7570	3.6128	3.5915	3.7161	4.2802	5.1436	5.3923	6.1164	4.4095
	MPE (%)	−0.6324	−1.3251	−0.7593	−0.4945	−0.8318	−0.4768	−0.5371	−0.6047	−0.7984	−0.6568	−1.0171	−1.1159	−0.6377
	R^2	0.9753	0.9773	0.9831	0.9820	0.9819	0.9833	0.9777	0.9830	0.9810	0.9806	0.9814	0.9794	0.9731
	ρ	0.9886	0.9893	0.9924	0.9918	0.9916	0.9925	0.9898	0.9924	0.9922	0.9912	0.9913	0.9903	0.9884
DWT-SSA-WNN	MSE (m/s)	0.0876	0.1040	0.0725	0.0548	0.0576	0.0676	0.0611	0.0609	0.0736	0.0837	0.0988	0.0727	0.0638
TR 80%	MAE (m/s)	0.2131	0.2268	0.1958	0.1694	0.1740	0.1843	0.1793	0.1769	0.1916	0.1998	0.2168	0.1898	0.1868
	$MAPE$ (%)	3.9857	5.4413	4.5362	3.6326	5.5075	3.5319	3.6285	3.6408	3.7108	4.8974	5.1147	5.7810	4.2037
	MPE (%)	−0.6140	−1.2651	−0.7123	−0.4812	−0.8099	−0.4974	−0.5191	−0.6052	−0.6427	−0.5974	−1.0011	−1.0765	−0.6361
	R^2	0.9776	0.9794	0.9850	0.9838	0.9838	0.9844	0.9773	0.9840	0.9855	0.9827	0.9836	0.9821	0.9760
	ρ	0.9899	0.9904	0.9935	0.9926	0.9925	0.9932	0.9897	0.9929	0.9938	0.9921	0.9925	0.9917	0.9897
DWT-SSA-WNN	MSE (m/s)	0.0798	0.0930	0.0666	0.0507	0.0539	0.0628	0.0607	0.0581	0.0687	0.0789	0.0928	0.0663	0.0591
TR 90%	MAE (m/s)	0.2045	0.2147	0.1874	0.1638	0.1682	0.1776	0.1785	0.1732	0.1839	0.1936	0.2101	0.1816	0.1804
	$MAPE$ (%)	3.8237	5.1475	4.3603	3.5189	5.3767	3.4118	3.6134	3.5582	3.5532	4.7233	4.9740	5.5448	4.0669
	MPE (%)	−0.5870	−1.2148	−0.7114	−0.4683	−0.7851	−0.4629	−0.5358	−0.5719	−0.6243	−0.5791	−0.9737	−1.0273	−0.6044
	R^2	0.9800	0.9815	0.9863	0.9851	0.9848	0.9855	0.9774	0.9848	0.9862	0.9836	0.9847	0.9837	0.9778
	ρ	0.9911	0.9914	0.9941	0.9932	0.9930	0.9937	0.9898	0.9934	0.9944	0.9927	0.9930	0.9925	0.9905

risk of overfitting. In contrast, lower decomposition levels yield a more generalised view of the signal. While this offers protection against noise, it runs the risk of overlooking pivotal signal patterns. Endpoint effects, often encountered in time series analysis, refer to potential discrepancies in predictive accuracy at the series' extremities. In the context of our DWT-prediction model combinations, we find that while such effects are discernible, their magnitude is subdued. Their influence on the overall predictive accuracy is minimal, attesting to the model's robustness across the entirety of the series.

Our results also emphasise the prowess of combining DWT with other techniques and selecting optimal hyperparameters. The comparative analysis, considering metrics like MAPE, underscores the efficiency of the DWT model when tuned with optimal hyperparameters, outclassing the performance achieved using a standard DB06 wavelet at level 4 decomposition. This observation reinforces the importance of hyperparameter tuning in wavelet-based methods. It is also intriguing to note that GPR and LSTM appear more sensitive to these hyperparameter changes than WNN and SVR.

Comparing the performance across various scenarios, a persistent theme is the superiority of the GPR model, especially when paired with DWT techniques. As gauged by metrics like MSE and MAPE, its consistent outperformance underscores its adaptability and robustness in handling the intricacies of wind speed time series. However, the improvements witnessed in SVR's performance when combined with DWT-SSA, specifically with a TR of 90%, are notable and shed light on the potential synergy between wavelet transformations and singular spectrum analysis. It is also essential to highlight the study's alignment with prior research, specifically with findings that established the effectiveness of coupling DWT with SSA. However, our research diverges in emphasising the edge that optimal DWT hyperparameters provide over the combined DWT-SSA approach, pointing towards the importance of individualised, data-driven hyperparameter selection in achieving enhanced prediction accuracy.

Our study underscores the pivotal role of meticulous hyperparameter selection and the tailored use of Daubechies wavelet orders in enhancing wind speed prediction accuracy. It also reinforces the importance of model selection, with certain models like GPR showcasing adaptability across different datasets and decomposition scenarios. The findings hold significance in emphasising the adaptability and nuanced understanding required in harnessing wavelet transforms for time series predictions.

Table 9
Error evaluation results of LSTM over all datasets.

Model	Evaluation criteria	DS01	DS02	DS03	DS04	DS05	DS06	DS07	DS08	DS09	DS10	DS11	DS12	DS13
LSTM	MSE (m/s)	0.6214	0.7698	0.5690	0.4145	0.4726	0.4653	0.4229	0.4273	0.4210	0.5805	0.7478	0.5970	0.4804
	MAE (m/s)	0.5675	0.6201	0.5452	0.4643	0.5060	0.4965	0.4777	0.4733	0.4595	0.5297	0.5973	0.5421	0.5091
	$MAPE$ (%)	10.8363	17.0686	13.1424	10.1258	16.5615	9.8998	10.0378	9.8249	9.6024	13.5840	14.6842	17.3600	12.7144
	MPE (%)	−2.4565	−7.2416	−3.5769	−2.1088	−5.5393	−2.0046	−2.2287	−1.6724	−2.4242	−4.3754	−4.6109	−6.5518	−4.3246
	R^2	0.8445	0.8487	0.8859	0.8811	0.8669	0.8890	0.8373	0.8870	0.9119	0.8787	0.8720	0.8544	0.8263
	ρ	0.9245	0.9263	0.9459	0.9431	0.9356	0.9488	0.9233	0.9469	0.9592	0.9421	0.9401	0.9288	0.9156
DWT-LSTM	MSE (m/s)	0.1481	0.1854	0.1293	0.0957	0.1100	0.1199	0.1078	0.1088	0.1153	0.1497	0.2001	0.1365	0.1085
(DB3, level 3)	MAE (m/s)	0.2768	0.3032	0.2596	0.2246	0.2401	0.2482	0.2359	0.2375	0.2381	0.2639	0.2972	0.2593	0.2409
	$MAPE$ (%)	5.2920	8.0340	6.3611	4.9752	8.0983	5.0322	4.8947	5.0481	5.0685	6.6498	7.1939	8.2341	5.9609
	MPE (%)	−0.7739	−2.2688	−1.1119	−0.7099	−1.6562	−0.8525	−0.5818	−0.7366	−0.7426	−1.1866	−1.3304	−1.7883	−1.3428
	R^2	0.9637	0.9635	0.9741	0.9723	0.9692	0.9718	0.9604	0.9721	0.9762	0.9696	0.9690	0.9669	0.9601
	ρ	0.9822	0.9823	0.9874	0.9866	0.9849	0.9864	0.9809	0.9865	0.9889	0.9853	0.9852	0.9838	0.9805
DWT-LSTM	MSE (m/s)	0.1271	0.1598	0.1088	0.0821	0.0938	0.1038	0.0915	0.0919	0.1015	0.1283	0.1877	0.1158	0.0911
(DB4, level 3)	MAE (m/s)	0.2550	0.2771	0.2367	0.2057	0.2195	0.2271	0.2165	0.2163	0.2206	0.2437	0.2764	0.2369	0.2202
	$MAPE$ (%)	4.8554	7.1268	5.7615	4.5515	7.3926	4.6360	4.5054	4.5937	4.6855	6.1303	6.6333	7.4539	5.3002
	MPE (%)	−0.6593	−1.8509	−1.0410	−0.6447	−1.3521	−0.7489	−0.6726	−0.7145	−0.8944	−1.0150	−1.3373	−1.6052	−1.0457
	R^2	0.9689	0.9689	0.9777	0.9761	0.9736	0.9760	0.9662	0.9761	0.9787	0.9742	0.9720	0.9716	0.9663
	ρ	0.9848	0.9851	0.9893	0.9886	0.9872	0.9886	0.9838	0.9886	0.9901	0.9876	0.9871	0.9861	0.9837
DWT-LSTM	MSE (m/s)	0.1227	0.1533	0.1051	0.0784	0.0931	0.0972	0.0899	0.0899	0.1007	0.1211	0.1872	0.1173	0.0887
(DB4, level 4)	MAE (m/s)	0.2486	0.2703	0.2324	0.2003	0.2171	0.2209	0.2125	0.2135	0.2138	0.2354	0.2706	0.2356	0.2170
	$MAPE$ (%)	4.7262	6.8837	5.6412	4.4101	7.2504	4.4268	4.3918	4.5397	4.3570	5.9396	6.4646	7.2337	5.0753
	MPE (%)	−0.5890	−1.6713	−0.9474	−0.5608	−1.1636	−0.5054	−0.5170	−0.6142	−0.6074	−1.0577	−0.9562	−1.2249	−0.8005
	R^2	0.9697	0.9698	0.9786	0.9773	0.9745	0.9774	0.9676	0.9770	0.9787	0.9757	0.9729	0.9722	0.9673
	ρ	0.9852	0.9853	0.9896	0.9889	0.9875	0.9891	0.9842	0.9888	0.9907	0.9882	0.9874	0.9865	0.9840
DWT-LSTM	MSE (m/s)	0.1033	0.1340	0.0914	0.0679	0.0758	0.0868	0.0802	0.0760	0.0826	0.1120	0.1683	0.0973	0.0759
(DB6, level 4)	MAE (m/s)	0.2340	0.2577	0.2183	0.1906	0.1988	0.2105	0.2004	0.1980	0.2031	0.2244	0.2575	0.2171	0.2020
	$MAPE$ (%)	4.4214	6.5426	5.2022	4.2066	6.5998	4.2546	4.0710	4.1681	4.1536	5.5172	6.1124	6.6842	4.7053
	MPE (%)	−0.5394	−1.5597	−0.7307	−0.4373	−1.0124	−0.4923	−0.4660	−0.6633	−0.5647	−0.7693	−0.8224	−1.1867	−0.7514
	R^2	0.9744	0.9739	0.9820	0.9805	0.9794	0.9799	0.9719	0.9809	0.9823	0.9784	0.9763	0.9774	0.9726
	ρ	0.9875	0.9876	0.9913	0.9905	0.9900	0.9905	0.9865	0.9909	0.9918	0.9895	0.9891	0.9890	0.9866
DWT-LSTM	MSE (m/s)	**0.0658**	**0.0881**	**0.0580**	**0.0436**	**0.0479**	**0.0558**	0.0499	**0.0506**	**0.0561**	**0.0699**	**0.1071**	0.0627	**0.0468**
Optimal	MAE (m/s)	**0.1873**	**0.2101**	**0.1760**	**0.1533**	**0.1595**	**0.1696**	**0.1604**	**0.1617**	**0.1659**	**0.1832**	**0.2197**	**0.1752**	**0.1590**
	$MAPE$ (%)	**3.5289**	5.0557	**4.2070**	**3.3878**	**5.3286**	**3.3873**	**3.2597**	3.4540	**3.4069**	**4.5618**	**5.3232**	5.4136	**3.7175**
	MPE (%)	**−0.2741**	−0.7845	**−0.4121**	−0.3322	−0.6045	**−0.2349**	−0.2245	−0.4018	**−0.3337**	**−0.4308**	**−0.7418**	**−0.5920**	−0.4444
	R^2	**0.9838**	**0.9828**	**0.9882**	**0.9874**	**0.9866**	**0.9870**	**0.9815**	**0.9871**	0.9882	**0.9856**	**0.9835**	**0.9855**	**0.9826**
	ρ	**0.9922**	**0.9919**	**0.9943**	**0.9939**	**0.9935**	**0.9939**	**0.9912**	**0.9939**	**0.9946**	**0.9931**	**0.9925**	**0.9930**	**0.9916**
DWT-SSA-LSTM	MSE (m/s)	0.0757	0.1013	0.0647	0.0492	0.0524	0.0600	0.0566	0.0592	0.0601	0.0781	0.1174	0.0691	0.0530
TR 10%	MAE (m/s)	0.1994	0.2226	0.1847	0.1618	0.1667	0.1736	0.1714	0.1711	0.1728	0.1934	0.2276	0.1842	0.1683
	$MAPE$ (%)	3.7388	5.2443	4.3959	3.5221	5.5630	3.4413	3.4742	3.6126	3.5376	4.8450	5.4932	5.6228	3.9059
	MPE (%)	−0.3622	**−0.7225**	−0.4808	−0.3627	−0.7415	−0.3511	−0.2245	−0.4294	−0.3764	−0.5300	−0.8017	−0.6626	−0.4462
	R^2	0.9811	0.9801	0.9872	0.9860	0.9851	0.9862	0.9793	0.9852	0.9875	0.9841	0.9821	0.9839	0.9804
	ρ	0.9908	0.9907	0.9938	0.9932	0.9928	0.9935	0.9900	0.9930	0.9943	0.9923	0.9919	0.9922	0.9905
DWT-SSA-LSTM	MSE (m/s)	0.0731	0.0949	0.0615	0.0470	0.0508	0.0583	0.0528	0.0547	0.0588	0.0742	0.1291	0.0663	0.0509
TR 70%	MAE (m/s)	0.1966	0.2159	0.1800	0.1595	0.1640	0.1724	0.1665	0.1655	0.1709	0.1887	0.2246	0.1819	0.1655
	$MAPE$ (%)	3.7240	5.0857	4.2810	3.4939	5.3778	3.4180	3.4101	3.4606	3.5170	4.7342	5.3681	5.5709	3.7888
	MPE (%)	−0.4689	−0.8833	−0.4767	**−0.3180**	−0.6449	−0.3101	−0.2181	−0.3425	−0.4984	−0.4402	−0.7849	−0.6985	**−0.3933**
	R^2	0.9815	0.9814	0.9876	0.9863	0.9859	0.9866	0.9802	0.9862	0.9875	0.9848	0.9817	0.9843	0.9811
	ρ	0.9911	0.9914	0.9940	0.9934	0.9932	0.9937	0.9904	0.9935	0.9945	0.9926	0.9919	0.9923	0.9908
DWT-SSA-LSTM	MSE (m/s)	0.0704	0.0908	0.0607	0.0463	0.0495	0.0572	0.0503	0.0526	0.0571	0.0725	0.1292	0.0641	0.0495
TR 80%	MAE (m/s)	0.1941	0.2128	0.1793	0.1584	0.1622	0.1712	0.1625	0.1635	0.1691	0.1878	0.2254	0.1779	0.1629
	$MAPE$ (%)	3.6551	5.0031	4.2607	3.4912	5.3451	3.4007	3.3087	3.4368	3.4998	4.7197	5.3813	5.4533	3.8330
	MPE (%)	−0.3060	−0.8107	−0.4700	−0.3270	−0.6180	−0.4278	**−0.1673**	−0.2638	−0.4553	−0.5629	−0.7698	−0.6755	−0.4641
	R^2	0.9822	0.9824	0.9878	0.9866	0.9862	0.9869	0.9814	0.9867	0.9880	0.9850	0.9820	0.9849	0.9818
	ρ	0.9914	0.9917	0.9941	0.9935	0.9933	0.9938	0.9910	0.9937	0.9944	0.9927	0.9921	0.9927	0.9911
DWT-SSA-LSTM	MSE (m/s)	0.0673	0.0893	0.0590	0.0455	0.0492	0.0569	**0.0496**	0.0510	0.0570	0.0732	0.1213	**0.0620**	0.0489
TR 90%	MAE (m/s)	0.1890	0.2116	0.1777	0.1566	0.1620	0.1713	0.1614	0.1620	0.1687	0.1861	0.2242	0.1760	0.1622
	$MAPE$ (%)	3.5799	**4.9754**	4.2550	3.4328	5.3669	3.4139	3.3103	**3.4222**	3.4709	4.7116	5.3652	**5.3830**	3.8185
	MPE (%)	−0.2895	−0.7942	−0.4863	−0.3270	**−0.5854**	−0.3395	−0.2194	**−0.2618**	−0.4490	−0.6231	−0.7711	−0.6494	−0.4578
	R^2	0.9833	0.9826	0.9881	0.9869	0.9862	0.9869	0.9812	0.9869	**0.9883**	0.9851	0.9827	0.9853	0.9820
	ρ	0.9920	0.9917	0.9943	0.9937	0.9933	0.9938	0.9910	0.9938	0.9946	0.9928	0.9922	0.9928	0.9913

Table 10
Comparison of prediction models using MSE and MAPE, normalized to persistence model performance.

	MSE					MAPE				
	Persistence	SVR	GPR	WNN	LSTM	Persistence	SVR	GPR	WNN	LSTM
Sole prediction	100.0%	107.0%	97.9%	140.4%	103.6%	100.0%	107.6%	99.7%	110.4%	104.0%
DWT (DB06, level4)		52.7%	11.3%	15.6%	18.5%		76.4%	31.3%	39.7%	43.1%
DWT (optimal)		47.7%	**5.2%**	**11.7%**	**11.9%**		73.2%	**19.5%**	**34.6%**	**34.9%**
DWT-SSA (Optimal + TR = 90%)		**44.1%**	6.5%	13.2%	12.3%		**70.2%**	23.4%	37.0%	35.4%

6. Conclusions

This study aims to investigate the impact of optimal hyperparameters for DWT and the combination of DWT and SSA on the performance of four different prediction models, namely SVR, GPR, WNN, and LSTM. The main objective is to enhance the accuracy of wind speed prediction, which plays a vital role in the efficient integration of wind power into the power grid. The results demonstrates that using optimal hyperparameters in the DWT model significantly improves the performance of various prediction models compared to Daubechies 6 (DB06) wavelet with level 4 decomposition. Our findings reveal that the optimal order of the Daubechies function for DWT is influenced by the prediction model used, and higher-order wavelets may be more suitable for some models like LSTM. Furthermore, the optimal decomposition levels of the DWT model are found to be predominantly between the third and fourth levels for most datasets and various prediction models. The performance of the combined DWT-SSA approach using TR 90% is also examined, and it is found that the optimal hyperparameters of DWT generally lead to superior results compared to the DWT-SSA approach. This observation not only improves the accuracy of wind speed forecasting but also reduces computational time.

This study highlights the importance of selecting appropriate hyperparameters for DWT and combining DWT with various prediction models to enhance the accuracy of wind speed prediction. The findings can contribute to the deeper penetration of wind energy into the

power grid by providing more accurate wind speed forecasts, which can help in optimising the scheduling and dispatch of wind power plants. Future research can explore the integration of additional preprocessing techniques, such as data denoising and feature selection, to further improve the accuracy of wind speed prediction models. Additionally, the investigation of other wavelet families and the development of custom wavelet functions tailored to specific prediction models or datasets could be valuable directions for future work.

CRediT authorship contribution statement

Ahmad Ahmad: Conceptualization, Methodology, Data curation, Coding, Simulation, Discussion, Writing – original draft. **Xun Xiao:** Supervision, Writing – review & editing. **Huadong Mo:** Supervision, Writing – review & editing. **Daoyi Dong:** Supervision, Writing – review & editing.

Declaration of competing interest

The authors declare that they have no known competing financial interests or personal relationships that could have appeared to influence the work reported in this paper.

Data availability

Data will be made available on request.

Acknowledgements

We would like to acknowledge the support of the National Energy Research Centre (NERC)/Royal Scientific Society (RSS) in Jordan for providing us with the datasets required for our study. Their contribution was important to the progress of our research.

References

Alexandridis, A.K., Zapranis, A.D., 2013. Wavelet neural networks: A practical guide. Neural Netw. 42, 1–27.
An, X., Jiang, D., Liu, C., Zhao, M., 2011. Wind farm power prediction based on wavelet decomposition and chaotic time series. Expert Syst. Appl. 38 (9), 11280–11285.
Ardalani-Farsa, M., Zolfaghari, S., 2010. Chaotic time series prediction with residual analysis method using hybrid Elman-NARX neural networks. Neurocomputing 73 (13–15), 2540–2553.
Bakos, G., 2009. Distributed power generation: a case study of small scale PV power plant in Greece. Appl. Energy 86 (9), 1757–1766.
Barbounis, T.G., Theocharis, J.B., Alexiadis, M.C., Dokopoulos, P.S., 2006. Long-term wind speed and power forecasting using local recurrent neural network models. IEEE Trans. Energy Convers. 21 (1), 273–284.
Blonbou, R., 2011. Very short-term wind power forecasting with neural networks and adaptive Bayesian learning. Renew. Energy 36 (3), 1118–1124.
Cadenas, E., Rivera, W., 2007. Wind speed forecasting in the south coast of Oaxaca, Mexico. Renew. Energy 32 (12), 2116–2128.
Cadenas, E., Rivera, W., 2009. Short term wind speed forecasting in La Venta, Oaxaca, México, using artificial neural networks. Renew. Energy 34 (1), 274–278.
Cadenas, E., Rivera, W., 2010. Wind speed forecasting in three different regions of Mexico, using a hybrid ARIMA-ANN model. Renew. Energy 35 (12), 2732–2738.
Castellani, F., Astolfi, D., Burlando, M., Terzi, L., 2015. Numerical modelling for wind farm operational assessment in complex terrain. J. Wind Eng. Ind. Aerodyn. 147, 320–329.
Castellani, F., Franceschini, G., 2005. A new technique to improve expected aep estimation in very complex terrain. In: 43rd AIAA Aerospace Sciences Meeting and Exhibit. p. 1331.
Catalão, J.d.S., Pousinho, H.M.I., Mendes, V.M.F., 2011. Short-term wind power forecasting in Portugal by neural networks and wavelet transform. Renew. Energy 36 (4), 1245–1251.
Chen, K., Yu, J., 2014. Short-term wind speed prediction using an unscented Kalman filter based state-space support vector regression approach. Appl. Energy 113, 690–705.
Chitsaz, H., Amjady, N., Zareipour, H., 2015. Wind power forecast using wavelet neural network trained by improved Clonal selection algorithm. Energy Convers. Manage. 89, 588–598.
Davò, F., Alessandrini, S., Sperati, S., Delle Monache, L., Airoldi, D., Vespucci, M.T., 2016. Post-processing techniques and principal component analysis for regional wind power and solar irradiance forecasting. Sol. Energy 134, 327–338.
Doucoure, B., Agbossou, K., Cardenas, A., 2016. Time series prediction using artificial wavelet neural network and multi-resolution analysis: Application to wind speed data. Renew. Energy 92, 202–211.
Elsner, J.B., Tsonis, A.A., 1996. Singular Spectrum Analysis: A New Tool in Time Series Analysis. Springer.
Frías-Paredes, L., Mallor, F., Gastón-Romeo, M., León, T., 2017. Assessing energy forecasting inaccuracy by simultaneously considering temporal and absolute errors. Energy Convers. Manage. 142, 533–546.
Golyandina, N., Nekrutkin, V., Zhigljavsky, A.A., 2001. Analysis of Time Series Structure: SSA and Related Techniques. CRC Press.
Graves, A., Liwicki, M., Fernández, S., Bertolami, R., Bunke, H., Schmidhuber, J., 2008. A novel connectionist system for unconstrained handwriting recognition. IEEE Trans. Pattern Anal. Mach. Intell. 31 (5), 855–868.
Han, J., Pei, J., Kamber, M., 2012. Data Mining: Concepts and Techniques. Elsevier.
Haque, A.U., Nehrir, M.H., Mandal, P., 2014. A hybrid intelligent model for deterministic and quantile regression approach for probabilistic wind power forecasting. IEEE Trans. Power Syst. 29 (4), 1663–1672.
Hu, J., Heng, J., Tang, J., Guo, M., 2018. Research and application of a hybrid model based on Meta learning strategy for wind power deterministic and probabilistic forecasting. Energy Convers. Manage. 173, 197–209.
Jaseena, K., Kovoor, B.C., 2020. A hybrid wind speed forecasting model using stacked autoencoder and LSTM. J. Renew. Sustain. Energy 12 (2), 023302.
Jawad, M., Ali, S.M., Khan, B., Mehmood, C.A., Farid, U., Ullah, Z., Usman, S., Fayyaz, A., Jadoon, J., Tareen, N., et al., 2018. Genetic algorithm-based non-linear auto-regressive with exogenous inputs neural network short-term and medium-term uncertainty modelling and prediction for electrical load and wind speed. J. Eng. 2018 (8), 721–729.
Jiang, P., Liu, Z., Niu, X., Zhang, L., 2021. A combined forecasting system based on statistical method, artificial neural networks, and deep learning methods for short-term wind speed forecasting. Energy 217, 119361.
Jones, L.E., 2017. Renewable Energy Integration: Practical Management of Variability, Uncertainty, and Flexibility in Power Grids. Academic Press.
Khosravi, A., Koury, R., Machado, L., Pabon, J., 2018. Prediction of wind speed and wind direction using artificial neural network, support vector regression and adaptive neuro-fuzzy inference system. Sustain. Energy Technol. Assess. 25, 146–160.
Kiplangat, D.C., Asokan, K., Kumar, K.S., 2016. Improved week-ahead predictions of wind speed using simple linear models with wavelet decomposition. Renew. Energy 93, 38–44.
Kumar, G., Malik, H., 2016. Generalized regression neural network based wind speed prediction model for western region of India. Procedia Comput. Sci. 93, 26–32.
Lei, C., Ran, L., 2008. Short-term wind speed forecasting model for wind farm based on wavelet decomposition. In: 2008 Third International Conference on Electric Utility Deregulation and Restructuring and Power Technologies. IEEE, pp. 2525–2529.
Lei, M., Shiyan, L., Chuanwen, J., Hongling, L., Yan, Z., 2009. A review on the forecasting of wind speed and generated power. Renew. Sustain. Energy Rev. 13 (4), 915–920.
Lerner, J., Grundmeyer, M., Garvert, M., 2009. The importance of wind forecasting. Renew. Energy Focus 10 (2), 64–66.
Li, Y., Wu, H., Liu, H., 2018. Multi-step wind speed forecasting using EWT decomposition, LSTM principal computing, RELM subordinate computing and IEWT reconstruction. Energy Convers. Manage. 167, 203–219.
Liu, H., Chen, C., 2019. Data processing strategies in wind energy forecasting models and applications: A comprehensive review. Appl. Energy 249, 392–408.
Liu, H., Mi, X., Li, Y., 2018. Smart multi-step deep learning model for wind speed forecasting based on variational mode decomposition, singular spectrum analysis, LSTM network and ELM. Energy Convers. Manage. 159, 54–64.
Liu, D., Niu, D., Wang, H., Fan, L., 2014. Short-term wind speed forecasting using wavelet transform and support vector machines optimized by genetic algorithm. Renew. Energy 62, 592–597.
Liu, H., Tian, H.-Q., Li, Y.-F., 2012. Comparison of two new ARIMA-ANN and ARIMA-Kalman hybrid methods for wind speed prediction. Appl. Energy 98, 415–424.
Liu, H., Tian, H.-Q., Pan, D.F., Li, Y.-F., 2013. Forecasting models for wind speed using wavelet, wavelet packet, time series and Artificial Neural Networks. Appl. Energy 107, 191–208.
Mallat, S.G., 1989. A theory for multiresolution signal decomposition: the wavelet representation. IEEE Trans. Pattern Anal. Mach. Intell. 11 (7), 674–693.
Mandal, P., Zareipour, H., Rosehart, W.D., 2014. Forecasting aggregated wind power production of multiple wind farms using hybrid wavelet-PSO-NNs. Int. J. Energy Res. 38 (13), 1654–1666.
Mi, X.-W., Liu, H., Li, Y.-F., 2017. Wind speed forecasting method using wavelet, extreme learning machine and outlier correction algorithm. Energy Convers. Manage. 151, 709–722.
Mi, X., Zhao, S., 2020. Wind speed prediction based on singular spectrum analysis and neural network structural learning. Energy Convers. Manage. 216, 112956.

Moreno, S.R., dos Santos Coelho, L., 2018. Wind speed forecasting approach based on singular spectrum analysis and adaptive neuro fuzzy inference system. Renew. Energy 126, 736–754.
Naik, J., Dash, S., Dash, P., Bisoi, R., 2018. Short term wind power forecasting using hybrid variational mode decomposition and multi-kernel regularized pseudo inverse neural network. Renew. Energy 118, 180–212.
Nayak, S., Misra, B.B., Behera, H.S., 2014. Impact of data normalization on stock index forecasting. Int. J. Comput. Inf. Syst. Ind. Manage. Appl. 6 (2014), 257–269.
Nielsen, H.A., Madsen, H., Nielsen, T.S., 2006. Using quantile regression to extend an existing wind power forecasting system with probabilistic forecasts. Wind Energy 9 (1–2), 95–108.
Palomares-Salas, J., De La Rosa, J., Ramiro, J., Melgar, J., Aguera, A., Moreno, A., 2009. ARIMA vs. Neural networks for wind speed forecasting. In: 2009 IEEE International Conference on Computational Intelligence for Measurement Systems and Applications. IEEE, pp. 129–133.
Pao, Y.-H., Park, G.-H., Sobajic, D.J., 1994. Learning and generalization characteristics of the random vector functional-link net. Neurocomputing 6 (2), 163–180.
Peng, T., Hubele, N., Karady, G., 1992. Advancement in the application of neural networks for short-term load forecasting. IEEE Trans. Power Syst. 7 (1), 250–257.
Ren, Y., Suganthan, P.N., Srikanth, N., Amaratunga, G., 2016. Random vector functional link network for short-term electricity load demand forecasting. Inform. Sci. 367, 1078–1093.
Saha, G., Chauhan, N., 2017. Numerical weather prediction using nonlinear auto regressive network for the Manaus region, Brazil. In: 2017 Innovations in Power and Advanced Computing Technologies (I-PACT). IEEE, pp. 1–4.
Santhosh, M., Venkaiah, C., Kumar, D.V., 2018. Ensemble empirical mode decomposition based adaptive wavelet neural network method for wind speed prediction. Energy Convers. Manage. 168, 482–493.
Singh, S., Mohapatra, A., et al., 2019. Repeated wavelet transform based ARIMA model for very short-term wind speed forecasting. Renew. Energy 136, 758–768.
Soman, S.S., Zareipour, H., Malik, O., Mandal, P., 2010. A review of wind power and wind speed forecasting methods with different time horizons. In: North American Power Symposium 2010. IEEE, pp. 1–8.
Sweeney, C., Bessa, R.J., Browell, J., Pinson, P., 2020. The future of forecasting for renewable energy. Wiley Interdiscip. Rev.: Energy Environ. 9 (2), e365.
Tascikaraoglu, A., Sanandaji, B.M., Poolla, K., Varaiya, P., 2016. Exploiting sparsity of interconnections in spatio-temporal wind speed forecasting using Wavelet Transform. Appl. Energy 165, 735–747.
Tayal, D., 2017. Achieving high renewable energy penetration in Western Australia using data digitisation and machine learning. Renew. Sustain. Energy Rev. 80, 1537–1543.
Wang, H., Lei, Z., Zhang, X., Zhou, B., Peng, J., 2019a. A review of deep learning for renewable energy forecasting. Energy Convers. Manage. 198, 111799.
Wang, Y., Wang, L., Chang, Q., Yang, C., 2020a. Effects of direct input–output connections on multilayer perceptron neural networks for time series prediction. Soft Comput. 24 (7), 4729–4738.
Wang, Y., Wang, H., Srinivasan, D., Hu, Q., 2019b. Robust functional regression for wind speed forecasting based on Sparse Bayesian learning. Renew. Energy 132, 43–60.
Wang, Y., Wang, J., Wei, X., 2015. A hybrid wind speed forecasting model based on phase space reconstruction theory and Markov model: A case study of wind farms in northwest China. Energy 91, 556–572.
Wang, C., Zhang, H., Ma, P., 2020b. Wind power forecasting based on singular spectrum analysis and a new hybrid Laguerre neural network. Appl. Energy 259, 114139.
Wang, S., Zhang, N., Wu, L., Wang, Y., 2016. Wind speed forecasting based on the hybrid ensemble empirical mode decomposition and GA-BP neural network method. Renew. Energy 94, 629–636.
Wu, Y.-K., Hong, J.-S., 2007. A literature review of wind forecasting technology in the world. In: 2007 IEEE Lausanne Power Tech. IEEE, pp. 504–509.
Wu, J.-G., Lundstedt, H., 1996. Prediction of geomagnetic storms from solar wind data using Elman recurrent neural networks. Geophys. Res. Lett. 23 (4), 319–322.
Xu, J., Liu, B., Mo, H., Dong, D., 2021. Bayesian adversarial multi-node bandit for optimal smart grid protection against cyber attacks. Automatica 128, 109551.
Xu, J., Sun, Q., Mo, H., Dong, D., 2022. Online routing for smart electricity network under hybrid uncertainty. Automatica 145, 110538.
Yin, H., Ou, Z., Huang, S., Meng, A., 2019. A cascaded deep learning wind power prediction approach based on a two-layer of mode decomposition. Energy 189, 116316.
Yu, C., Li, Y., Zhang, M., 2017. An improved wavelet transform using singular spectrum analysis for wind speed forecasting based on Elman neural network. Energy Convers. Manage. 148, 895–904.
Zhang, W., Lin, Z., Liu, X., 2022a. Short-term offshore wind power forecasting-A hybrid model based on Discrete Wavelet Transform (DWT), Seasonal Autoregressive Integrated Moving Average (SARIMA), and deep-learning-based Long Short-Term Memory (LSTM). Renew. Energy 185, 611–628.
Zhang, C., Peng, T., Nazir, M.S., 2022b. A novel hybrid approach based on variational heteroscedastic Gaussian process regression for multi-step ahead wind speed forecasting. Int. J. Electr. Power Energy Syst. 136, 107717.
Zhang, W., Wang, J., Wang, J., Zhao, Z., Tian, M., 2013. Short-term wind speed forecasting based on a hybrid model. Appl. Soft Comput. 13 (7), 3225–3233.
Zhang, C., Wei, H., Zhao, X., Liu, T., Zhang, K., 2016. A Gaussian process regression based hybrid approach for short-term wind speed prediction. Energy Convers. Manage. 126, 1084–1092.
Zhao, X., Wang, S., Li, T., 2011. Review of evaluation criteria and main methods of wind power forecasting. Energy Procedia 12, 761–769.